

Non-smooth variational regularization for processing manifold-valued data

M. Holler and A. Weinmann

September 20, 2019

Abstract

Many methods for processing scalar and vector valued images, volumes and other data in the context of inverse problems are based on variational formulations. Such formulations require appropriate regularization functionals that model expected properties of the object to reconstruct. Prominent examples of regularization functionals in a vector-space context are the total variation (TV) and the Mumford-Shah functional, as well as higher-order schemes such as total generalized variation models. Driven by applications where the signals or data live in nonlinear manifolds, there has been quite some interest in developing analogous methods for nonlinear, manifold-valued data recently. In this chapter, we consider various variational regularization methods for manifold-valued data. In particular, we consider TV minimization as well as higher order models such as total generalized variation (TGV). Also, we discuss (discrete) Mumford-Shah models and related methods for piecewise constant data. We develop discrete energies for denoising and report on algorithmic approaches to minimize them. Further, we also deal with the extension of such methods to incorporate indirect measurement terms, thus addressing the inverse problem setup. Finally, we discuss wavelet sparse regularization for manifold-valued data.

1 Introduction

Any measurement process, either direct or indirect, produces noisy data. While for some setups, the noise can safely be ignored, for many others it severely hinders an interpretation or further processing of the data of interest. In addition, measurements might also be incomplete such that again direct usability of the measured data is limited.

Variational regularization, i.e., a postprocessing or reconstruction of the quantity of interest via the minimization of an energy functional, often allows to reduce data corruption significantly. The success of such methods heavily relies on suitable regularization functionals and, in particular in the broadly relevant situation that the quantity of interest is sparse in some sense, non-smooth functionals are known to perform very well. Prominent and well-established examples of non-smooth regularization functional in the context of vector-space data are for instance the total variation functional and higher-order extensions such as total generalized variation, the Mumford-Shah functional and the ℓ^1 - or ℓ^0 -penalization of coefficients w.r.t. some wavelet basis.

When it comes to data in a non-linear space such as a manifold, the situation is different and the development of appropriate analogues of non-smooth regularization functionals in this setting is currently an active topic of research with many challenges still to be overcome. Most of these challenges are related to the nonlinearity of the underlying space, which complicates the transfer of concepts from the context of vector-space regularizers, such as measure-valued derivatives or basis transforms, but also their numerical realization.

On the other hand, applications where the underlying data naturally lives in a non-linear space are frequent and relevant. A prominent example is diffusion tensor imaging (DTI), which is a technique to quantify non-invasively the diffusional characteristics of a specimen [10, 69]. Here the underlying data space is the set of positive (definite) matrices, which becomes a Cartan-Hadamard manifold when equipped with the corresponding Fisher-Rao metric. Another example is interferometric synthetic aperture radar (InSAR) imaging, which is an important airborne imaging modality for geodesy [76]. Often the InSAR image has the interpretation of a wrapped periodic version of a digital elevation model [87] and the underlying data space is the unit circle \mathbb{S}^1 . Further examples are nonlinear color spaces for image processing, as for instance the LCh, HSV and HSL color spaces (where the underlying manifold is the cylinder $\mathbb{R}^2 \times \mathbb{S}^1$) and chromaticity-based color spaces where the underlying manifold is $\mathbb{S}^2 \times \mathbb{R}$, see [37]. Also, the rotation group $\text{SO}(3)$ appears as data space in the context of aircraft orientations and camera positions [105], protein alignments [60], and the tracking of 3D rotational data arising in robotics [44]. Data in the euclidean motion group $\text{SE}(3)$ may represent poses [89] and sphere-valued data appear as orientation fields of three dimensional images [86]. Finally, shape-space data [77, 16] constitutes manifold-valued data as well.

Motivated by such applications, we review existing non-smooth regularization techniques for non-linear geometric data and their numerical realization in this chapter. Following the majority of existing approaches, we will concentrate on discrete signals in a finite difference setting, which is appropriate particularly for image processing tasks due to the mostly Cartesian grid domains of images. We start with total variation regularization in Section 2, which can be transferred to a rather simple yet effective approach for non-linear data with different possibilities for a numerical realization. With the aim of overcoming well-known drawbacks of TV regularization, in particular so-called staircasing effects, we then move to higher-order functionals in Section 3, where the goal is to provide a model for piecewise smooth data with jumps. Next, having a similar scope, we discuss different models for Mumford-Shah regularization and their algorithmic realization (using concepts of dynamic programming) in Section 4. Indirect measurements in the context of manifold valued data are then the scope of Section 5, where we consider a regularization framework and algorithmic realization that applies to the previously defined approaches. Finally, we deal with wavelet sparse regularization of manifold valued data in Section 6 where we consider ℓ^1 and ℓ^0 type models and their algorithmic realization.

2 Total Variation Regularization of Manifold Valued Data

For scalar data, total variation regularization was early considered by Rudin, Osher and Fatemi [90] and by Chambolle and Lions [34] in the 1990s. A major advantage of total variation regularization compared to classical Tikhonov regularization is that it preserves sharp edges [101, 59] which is the reason for a high popularity of TV regularization in particular in applications with image-related data. The most direct application of TV regularization is denoising, where ℓ^2 data terms have originally been used in [90] (and are well-suited in case of Gaussian noise) and ℓ^1 data terms are popular due to robustness against outliers and some favorable analytical properties [3, 81, 36]. An extension of TV for vector-valued data has early been considered in [91] and we refer to [45] for an overview of different approaches.

This section reviews existing extensions of TV regularization to manifold-valued data. In the continuous setting, such an extension has been considered analytically in [57, 56], where [56] deals with the \mathbb{S}^1 case and [57] deals with the general case using the notion of cartesian currents. There, in particular, the existence of minimizers of certain TV-type energies in the continuous domain setup has been shown. In a discrete, manifold-valued setting, there is a rather

straight forward definition of TV. Here, the challenge is more to develop appropriate algorithmic realizations. Indeed, many of the successful numerical algorithms for TV minimization in the vector space setting, such as [32, 35, 58] and [82] for ℓ^1 -TV, rely on smoothing or convex duality, where for the latter no comprehensive theory is available in the manifold setting.

2.1 Models

For univariate data of length N in a finite dimensional Riemannian manifold \mathcal{M} , the (discrete) TV denoising problem with ℓ^q -type data fidelity term reads as

$$\operatorname{argmin}_{x \in \mathcal{M}^N} \left\{ \frac{1}{q} \sum_{i=1}^N d(x_i, f_i)^q + \alpha \sum_{i=1}^{N-1} d(x_i, x_{i+1}) \right\}. \quad (1)$$

Here, $f = (f_i)_{i=1}^N$ denotes the observed data and $x = (x_i)_{i=1}^N$ is the argument to optimize for. Further, $q \in [1, \infty)$ is a real number and $\alpha > 0$ is a regularization parameter controlling the trade of between data fidelity and the regularity. The symbol $d(y, z)$ denotes the distance induced by the Riemannian metric on the manifold \mathcal{M} . We note that in the euclidean case $\mathcal{M} = \mathbb{R}^d$, the above distance to the data f corresponds to the ℓ^q norm. For noise types with heavier tails (such as Laplacian noise in the euclidean case,) $q = 1$ is a good choice. We further point out that, in the scalar case $\mathcal{M} = \mathbb{R}$, the expression $\sum_{i=1}^{N-1} d(x_i, x_{i+1})$ defines the total variation of the sequence x interpreted as a finite sum of point measures.

In the bivariate case, a manifold version of TV denoising for signals in $\mathcal{M}^{N \times M}$ is given by

$$\operatorname{argmin}_{u \in \mathcal{M}^{N \times M}} \left\{ \frac{1}{q} \sum_{i,j} d(x_{i,j}, f_{i,j})^q + \alpha \sum_{i,j} (d(x_{i,j}, x_{i+1,j})^p + d(x_{i,j}, x_{i,j+1})^p)^{1/p} \right\}. \quad (2)$$

Note that here and on the following, we will frequently omit the index bounds in finite-length signals and sums for the sake of simplicity, and always implicitly set all scalar-valued summands containing out-of-bound indices to 0. In (2), the cases $p = 1$ and $p = 2$ are most relevant, where $p = 1$ has computational advantages due to a separable structure and $p = 2$ is often used because it corresponds to an isotropic functional in the continuous, vector-space case. We note however that, in the TV case, the effects resulting from anisotropic discretization are not severe. Moreover, they can be almost completely eliminated by including further difference directions, such as diagonal differences. For details on including further difference directions we refer to Section 4 (discussing reduction of anisotropy effects for the Mumford-Shah case in which case such effects are more relevant.)

Note that if we replace the distance term in the TV component of (1) by the squared distance (or remove the square root for $p = 2$ in (2)), we end up with a discrete model of classical H^1 regularization. Further, we may also replace the distance term in the regularizer by $h \circ d$ where h can for instance be the so-called Huber function which is a parabola for small arguments smoothly glued with two linear functions for larger arguments. Using this, we end up with models for Huber regularization, see [116] for details.

2.2 Algorithmic Realization

As mentioned in the introduction to this section, the typical methods used for TV regularization in vector spaces are based on convex duality. The respective concepts are not available in a manifold setting. However, there are different strategies to solve (1) and (2), and we briefly review some relevant strategies in the following.

The authors of [100, 40] consider TV regularization for \mathbb{S}^1 -valued data and develop a lifting approach, i.e., they lift functions with values in \mathbb{S}^1 to functions with values in the universal covering \mathbb{R} of \mathbb{S}^1 , lifting the involved functionals at the same time such that periodicity of the data is respected. This results in a nonconvex problem for real valued data (which still reflects the original \mathbb{S}^1 situation), which can then algorithmically be approached by using convex optimization techniques on the convex relaxation of the nonconvex vector space problem. We note that the approach is a covering space approach which relies on the fact that the covering space is a vector space which limits its generalization to general manifolds. In connection with \mathbb{S}^1 valued data we also point out the paper [98] which provides an exact solver for the univariate L^1 -TV problem (1) with $q = 1$.

For general manifolds there are three conceptually different approaches to TV regularization. The authors of [74] reformulate the TV problem as a multi-label optimization problem. More precisely, they consider a lifted reformulation in a vector-space setting, where the unknown takes values in the space of probability measures on the manifold (rather than the manifold itself), such that it assigns a probability for each given value on the manifold. Constraining the values of the unknown to be delta peaks, this would correspond to an exact reformulation whereas dropping this constraint yields a convex relaxation. After discretization, the unknown takes values in the unit simplex assigning a probability to each element of a discrete set of possible values. This corresponds to a lifting of the problem to higher dimensions, where the number of values the unknown is allowed to attain defines the dimensionality of the problem. Having a vector-space structure available, the lifted problem is then solved numerically using duality-based methods. We refer to [74] for details and to [107] for an overview of research in that direction and extensions.

Another approach can be found in the paper [63]. There, the authors employ an iteratively reweighted least squares (IRLS) algorithm to the isotropic discrete TV functional (2). The idea of the IRLS is to replace the distance terms in the TV regularizer by squared distance terms and to introduce a weight for each summand of the regularizer. Then, fixing the weights, the problem is differentiable and can be solved using methods for differentiable functions such as a gradient descent scheme. In a next step, the weights are updated where a large residual part of a summand results in a small weight, and the process is iterated. This results in an alternating minimization algorithm. The authors show convergence in the case of Hadamard spaces and for data living in a half-sphere. We mention that IRLS minimization is frequently applied for recovering sparse signals and that it has been also applied to scalar TV minimization in [88]. In connection with this, we also mention the paper [13] which considers half-quadratic minimization approaches that are generalizations of [63].

Finally, the approach of [116] to TV regularization employs iterative geodesic averaging to implement cyclic and parallel proximal point algorithms. The main point here is that the appearing proximal mappings can be analytically computed and the resulting algorithms exclusively perform iterative geodesic averaging. This means that only points on geodesics have to be computed. We will elaborate on this approach in the following. In connection with this, we also mention the paper [12] where a generalized forward-backward type algorithm is proposed to solve a related problem in the context of DTI; see also [11, 92] in the context of shape spaces.

The approach of [116] relies on the concepts of cyclic proximal point algorithms (CPPAs) and parallel proximal point algorithms (PPPA) in a manifold. A reference for cyclic proximal point algorithms in vector spaces is [19]. In the context of nonlinear spaces, the concept of CPPAs was first proposed in [7], where it is employed to compute means and medians in Hadamard spaces. In the context of variational regularization methods for nonlinear, manifold-valued data, they were first used in [116], which also proposed the PPPA in the manifold setting.

CPPAs and PPPAs. The idea of both CPPAs and PPPAs is to decompose a functional

Algorithm 1 CPPA for solving $\min_x F(x)$ with $F = \sum_{j=1}^K F_j$

```

1: CPPA( $x^0, (\lambda_k)_k, (\sigma(j))_{j=1}^K$ )
2:  $k = 0, x_0^0 = x^0$ 
3: repeat until stopping criterion fulfilled
4:   for  $j = 1, \dots, K$ 
5:      $x_j^k = \text{prox}_{\lambda_k F_{\sigma(j)}}(x_{j-1}^k)$ 
6:    $x_0^{k+1} = x_K^k, \quad k \leftarrow k + 1$ 
7: return  $x_0^k$ 

```

Algorithm 2 PPPA for solving $\min_x F(x)$ with $F = \sum_{j=1}^K F_j$

```

1: PPPA( $x^0, (\lambda_k)_k$ )
2:  $k = 0,$ 
3: repeat until stopping criterion fulfilled
4:   for  $j = 1, \dots, K$ 
5:      $x_j^{k+1} = \text{prox}_{\lambda_k F_j}(x^k)$ 
6:    $x^{k+1} = \text{mean}_j(x_j^{k+1}), \quad k \leftarrow k + 1$ 
7: return  $x^k$ 

```

$F : \mathcal{M}^N \rightarrow \mathbb{R}$ to be minimized into basic atoms $(F_i)_{i=1}^K$ and then to compute the proximal mappings of the atoms F_i iteratively. For a CPPA, this is done in a cyclic way, and for a PPPA, in a parallel way. More precisely, assume that

$$F = \sum_{i=1}^K F_i \quad (3)$$

and consider the proximal mappings [78, 48, 6] $\text{prox}_{\lambda F_i} : \mathcal{M}^N \rightarrow \mathcal{M}^N$ given as

$$\text{prox}_{\lambda F_i}(x) = \underset{y}{\text{argmin}} F_i(y) + \frac{1}{2\lambda} \sum_{j=1}^N d(x_j, y_j)^2. \quad (4)$$

One cycle of a CPPA then consists of applying each proximal mapping $\text{prox}_{\lambda F_i}$ once in a pre-scribed order, e.g., $\text{prox}_{\lambda F_1}, \text{prox}_{\lambda F_2}, \text{prox}_{\lambda F_3}, \dots$, or, generally, $\text{prox}_{\lambda F_{\sigma(1)}}, \text{prox}_{\lambda F_{\sigma(2)}}, \text{prox}_{\lambda F_{\sigma(3)}}, \dots$, where the symbol σ is employed to denote a permutation. The cyclic nature is reflected in the fact that the output of $\text{prox}_{\lambda F_{\sigma(i)}}$ is used as input for $\text{prox}_{\lambda F_{\sigma(i+1)}}$. Since the i th update is immediately used for the $(i+1)$ th step, it can be seen as a Gauss-Seidel-type scheme. We refer to Algorithm 1 for its implementation in pseudocode.

A PPPA consists of applying the proximal mapping to each atom F_i to the output of the previous iteration x^k in parallel and then averaging the results, see Algorithm 2. Since it performs the elementary update steps, i.e., the evaluation of the proximal mappings, in parallel it can be seen as update pattern of Jacobi type. In Algorithm 2, the symbol *mean* denotes the generalization of the arithmetic average to a Riemannian manifold, which is the well known intrinsic mean, i.e., given z_1, \dots, z_K in \mathcal{M} , a mean $z^* \in \mathcal{M}$ is defined by (cf. [70, 71, 83, 50])

$$z^* = \text{mean}_j(z_j) = \underset{z \in \mathcal{M}}{\text{argmin}} \sum_{j=1}^K d(z, z_j)^2. \quad (5)$$

Please note that this definition is employed component-wise for x^{k+1} in Algorithm 2. We note that, if the $(F_i)_i$ are lower semi continuous, both the minimization problem for the proximal

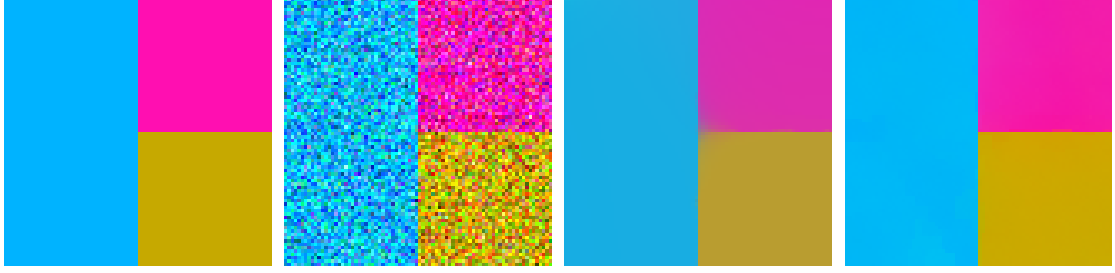


Figure 1: The effect of ℓ^2 -TV denoising in LCh space ($\alpha = 0.80$). *Left.* Ground truth. *Middle left.* Noisy input image corrupted by Gaussian noise on each channel. *Middle right.* The ℓ^2 -TV reconstruction in linear space. *Right.* The ℓ^2 -TV reconstruction in the nonlinear LCh color space. Using the distance in the non-flat LCh metric can lead to higher reconstruction quality.

mapping and for the mean admit a solution. On general manifolds, however, the solution is not necessarily unique. For arguments whose points are all contained in a small ball (whose radius depends on the sectional curvature \mathcal{M}) it is unique, see [48, 6, 71, 70] for details. This is a general issue in the context of manifolds that are – in a certain sense – a local concept involving objects that are often only locally well defined. In case of ambiguities, we hence consider the above objects as set-valued quantities.

During the iteration of both CPPA and PPPA, the parameter λ_k of the proximal mappings is successively decreased. In this way, the penalty for deviation from the previous iterate is successively increased. It is chosen in a way such that the sequence $(\lambda^k)_k$ is square-summable but not summable. Provided that this condition holds, the CPPA can be shown to converge to the optimal solution of the underlying minimization problem, at least in the context of Hadamard manifolds and convex $(F_i)_i$, see [8, Theorem 3.1]. The same statement holds for the PPPA, see [116, Theorem 4]. The mean can be computed using a gradient descent or a Newton scheme. To reduce the computation time further, it has been proposed in [116] to replace the mean by another construction (known as geodesic analogues in the subdivision context [109]) which is an approximation of the mean that is computationally less demanding. As above, in the context of Hadamard manifolds and convex $(F_i)_i$, the convergence towards a global minimizer is guaranteed, see [116, Theorem 7]. For details we refer to the above reference.

Proximal mappings for the atoms of the TV functions. Now we consider a splitting of the univariate problem (1) and the bivariate problem (2) into basic atoms such that the CPPA and the PPPA can be applied. Regarding (1) we use the atoms

$$F_1(x) := \frac{1}{q} \sum_{i=1}^N d(x_i, f_i)^q, \quad F_2(x) = \sum_{\substack{i=1 \\ i \text{ odd}}}^{N-1} d(x_i, x_{i+1}), \quad F_3(x) = \sum_{\substack{i=1 \\ i \text{ even}}}^N d(x_i, x_{i+1}). \quad (6)$$

Regarding (2), we consider the case $p = 1$ and again define F_1 to be the data term, F_2 and F_3 to be a splitting of the sum $\sum_{i,j} d(x_{i,j}, x_{i+1,j})$ into even and odd values of i and F_4 and F_5 to be a splitting of the sum $\sum_{i,j} d(x_{i,j}, x_{i,j+1})$ into even and odd values of j . With these splittings, all summands in the atom $(F_i)_i$ decouple such that the computation of the proximal mappings reduces to a point-wise computation of the proximal mappings of

$$x \mapsto g_1(x, f) := \frac{1}{q} d(x, f)^q \quad \text{and} \quad (x_1, x_2) \mapsto g_2(x_1, x_2) = d(x_1, x_2). \quad (7)$$

From the splitting (6) (and its bivariate analogue below (6)) together with (7) we see that within a PPPA all proximal mappings of the basic building blocks g_1, g_2 can be computed in parallel

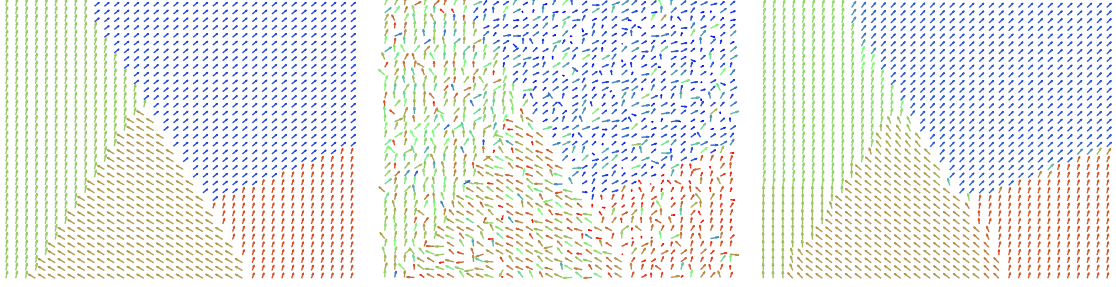


Figure 2: Denoising of an \mathbb{S}^2 -valued image. The polar angle is coded both as length of the vectors and as color (red pointing towards the reader, blue away from the reader). *Left.* Synthetic image. *Center.* Noisy data (corrupted by von Mises-Fisher noise of level $\kappa = 5.5$). *Right.* ℓ^2 -TV regularization using $\alpha = 0.7$. The noise is almost completely removed whereas the jumps are preserved.

and the computation of each mean only involves 3 points in the manifold \mathcal{M} in the univariate setting and 5 points in the multivariate setting. For a CPPA we see that a cycle has length 3 and 5 in the univariate and bivariate situation, respectively, and that within each atom F_i the proximal mappings of the respective terms of the form g_1, g_2 can be computed in parallel.

For the data term, the proximal mappings $\text{prox}_{\lambda g_1}$ are explicit for $q = 1$ and $q = 2$ and, as derived in [48], are given as

$$(\text{prox}_{\lambda g_1(\cdot, f)})_j(x) = [x, f]_t \quad (8)$$

where

$$t = \frac{\lambda}{1+\lambda} \quad \text{for } q = 2, \quad t = \min\left(\frac{\lambda}{d(x, f)}, 1\right) \quad \text{for } q = 1. \quad (9)$$

Here, we use the symbol $[\cdot, \cdot]_t$ to denote the point reached after time t on the (non unit speed) length-minimizing geodesic starting at the first argument reaching the second argument at time 1. (Note, that up to sets of measure zero, length minimizing geodesics are unique, and in the extraordinary case of non-uniqueness we pick may one of them.)

Regarding g_2 , it is shown in [116] that the proximal mappings are given in closed form as

$$\text{prox}_{\lambda g_2}((x_1, x_2)) = ([x_1, x_2]_t, [x_2, x_1]_t), \quad \text{where } t = \min\left(\frac{\lambda \alpha}{d(x_1, x_2)}, \frac{1}{2}\right). \quad (10)$$

Here, for each point, the result is a point on the geodesic segment connecting two arguments.

It is important to note that the point $p_t = [p_0, p_1]_t$ on the geodesic connecting two points p_0, p_1 is given in terms of the Riemannian exponential map \exp and its inverse denoted by \log or \exp^{-1} by

$$p_t = [p_0, p_1]_t = \exp_{p_0}(t \log_{p_0} p_1). \quad (11)$$

Here, $v := \log_{p_0} p_1$ denotes that tangent vector sitting in p_0 such that $\exp_{p_0} v = p_1$. The tangent vector v is scaled by t , and then the application of the \exp -map yields p_t . More precisely, \exp_{p_0} assigns the point $p_t = \exp_{p_0} tv$ to the tangent vector tv by evaluating the geodesic starting in p_0 with tangent vector tv at time 1.

We note that also the proximal mappings of the classical Tichanov regularizers as well as of the Huber regularizers mentioned above have a closed form representation in terms of geodesic averaging as well. Further, there are strategies to approximate intrinsic means by iterated geodesic

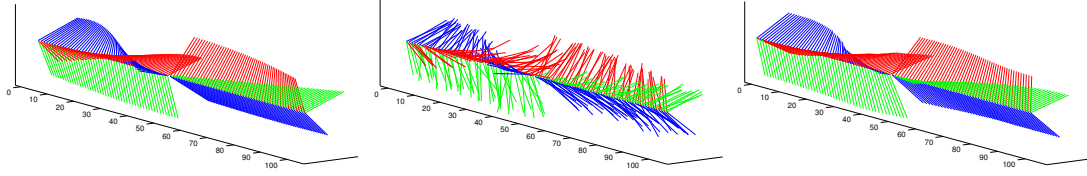


Figure 3: Result (*right*) of denoising an $\text{SO}(3)$ -valued noisy time-series (*center*) using the inexact parallel algorithm for L^2 -TV regularization with $\alpha = 4.0$. (*Left:* Ground truth.) Here, an element of $\text{SO}(3)$ is visualized by the rotation of a tripod. We observe that the noise is removed and the jump is preserved.

averages to speed up the corresponding computations. For details on these comments we refer to [116].

Plugging in the splittings and proximal mappings as above into the Algorithms 1 and 2 yields a concrete implementation for the TV-regularized denoising of manifold-valued data. Regarding convergence, we have the following result.

Theorem 1. *For data in a (locally compact) Hadamard space and a parameter sequence $(\lambda_k)_k$ which is squared summable but not summable, the iterative geodesic averaging algorithms for TV-regularized denoising (based on the CPPA, the PPPA, as well as the inexact approximative and fast variant of the PPPA) converge towards a minimizer of the ℓ^p -TV functional.*

We further remark that the statement remains true when using the Huber potential mentioned above either as data term or for the regularization, as well as when using quadratic variation instead of TV. A proof of this statement and more details on the remarks can be found in [116].

We illustrate the algorithms with some examples. First we consider denoising in the LCh color space. As explained above, the underlying manifold is $\mathbb{S}^1 \times \mathbb{R}^2$. The exponential and its inverse are given componentwise by the respective mappings on \mathbb{R}^2 and \mathbb{S}^1 . By (11), this allows to compute the involved proximal mappings via (8), (9) and (10), respectively. We point out that in spite of the separability of the exponential and its inverse, the proposed algorithm is in general not equivalent to performing the algorithm on \mathbb{R}^2 and \mathbb{S}^1 separately. The reason is that the parameter t in (9) and (10) depend nonlinearly on the distance in the product manifold (except for $p, q = 2$). In Figure 1 we illustrate the denoising potential of the proposed scheme in the LCh space. Here, the vector-space computation was realized using the split Bregman method for vectorial TV regularization [58, 55] and we optimized the parameters of both methods with respect to the peak signal to noise ratio.

As a second example we consider noisy data on the unit sphere \mathbb{S}^2 (in \mathbb{R}^3). In Figure 2, we test the denoising potential of our algorithm on a noisy (synthetic) spherical-valued image. As noise model on \mathbb{S}^2 , we use the von Mises-Fisher distribution having the probability density $h(x) = c(\kappa) \exp(\kappa x \cdot \mu)$. Here, $\kappa > 0$ expresses the concentration around the mean orientation $\mu \in \mathbb{S}^2$ where a higher κ indicates a higher concentration of the distribution and $c(\kappa)$ is a normalization constant. We observe in Figure 2 that the noise is almost completely removed by TV minimization and that the edges are retained.

In Figure 3 we consider an univariate signal with values in the special orthogonal group $\text{SO}(3)$ consisting of all orthogonal 3×3 matrices with determinant one. We see that the proposed algorithm removes the noise and that the jump is preserved. Finally, we consider real InSAR data [76, 87] in Figure 4. InSAR images consist of phase values such that the underlying manifold is the one-dimensional sphere \mathbb{S}^1 . The image is taken from [87]. We apply total variation denoising



Figure 4: Total variation denoising of an \mathbb{S}^1 -valued InSAR image (real data, *left*) using L^2 -TV regularization ($\alpha=0.32$, *middle*) and L^1 -TV regularization ($\alpha=0.60$, *right*). Here, the circle \mathbb{S}^1 is represented as an interval with endpoints identified, i.e., white and black represent points nearby. Total variation minimization reliably removes the noise while preserving the structure of the image.

using ℓ^2 and ℓ^1 data terms. We observe that TV regularization reduces the noise significantly. The ℓ^1 data term seems to be more robust to outliers than the ℓ^2 data term.

3 Higher Order Total Variation Approaches, Total Generalized Variation

It is well known in the vector space situation (and analytically confirmed for instance in [24, 21]) that TV regularization has a tendency to produce piecewise-constant results, leading to artificial jump discontinuities in case of ground truth data with smooth regions. Classical H^1 regularization avoids this effect. However, H^1 regularity does not allow for jump discontinuities, which can be seen as motivation for considering non-smooth higher order approaches. While second order TV regularization [41, 65], i.e., penalizing the Radon norm of the second order distributional derivative of a function, is a first attempt in this direction, one can show that functions whose second order distributional derivative can be represented by a Radon measure again cannot have jumps along (smooth) hypersurfaces [25]. This disadvantage is no longer present when using a combination of first and second order TV via infimal convolution, i.e.,

$$\text{IC}_\alpha(u) = \inf_v \alpha_1 \text{TV}(u - v) + \alpha_0 \text{TV}^2(v),$$

as originally proposed in [34]. Here, $\alpha = (\alpha_1, \alpha_0) \in (0, \infty)^2$ are two weights. Regularization with TV-TV² infimal convolution finds an optimal additive decomposition of the unknown u in two components, where one yields minimal cost for TV and the other one for second order TV. Extending on that, the (second order) total generalized variation (TGV) functional [28] optimally balances between first and second order derivatives on the level of the gradient rather than the function, i.e., is given as

$$\text{TGV}_\alpha^2(u) = \inf_w \alpha_1 \|\nabla u - w\|_{\mathcal{M}} + \alpha_0 \|\mathcal{E}w\|_{\mathcal{M}},$$

where $\mathcal{E}w = 1/2(Jw + Jw^T)$ is a symmetrization of the Jacobian matrix field Jw and again $\alpha = (\alpha_1, \alpha_0) \in (0, \infty)^2$ are two weights. This provides a more flexible balancing between different orders of differentiation and, in particular in situations when an optimal decomposition on the

image level is not possible, further reduces piecewise constancy artifacts still present with TV-TV² infimal convolution, see [28].

Motivated by the developments for vector spaces, and due to the challenges appearing when extending them to manifold-valued data, several works deal with developing non-smooth higher order regularization in this setting. In the following we motivate and review some existing approaches and strive to present them in a common framework. Following the existing literature, we consider a discrete setting.

3.1 Models

First, we define the above-mentioned higher order regularization functionals in a discrete, vector-space setting. To this aim, for $u = (u_{i,j})_{i,j} \in \mathbb{R}^{N \times M}$, let $\delta_x : \mathbb{R}^{N \times M} \rightarrow \mathbb{R}^{(N-1) \times M}$, $(\delta_x u)_{i,j} = u_{i+1,j} - u_{i,j}$ and $\delta_y : \mathbb{R}^{N \times M} \rightarrow \mathbb{R}^{N \times (M-1)}$, $(\delta_y u)_{i,j} = u_{i,j+1} - u_{i,j}$ be finite differences (on a staggered grid to avoid boundary effects) w.r.t. the first- and second component, respectively. A discrete gradient, Jacobian and symmetrized Jacobian are then given as

$$\begin{aligned}\nabla u &= (\delta_x u, \delta_y u), & J(v^1, v^2) &= (\delta_x v^1, \delta_y v^2, \delta_y v^1, \delta_x v^2), \\ \mathcal{E}(v^1, v^2) &= (\delta_x v^1, \delta_y v^2, \frac{\delta_y v^1 + \delta_x v^2}{2}),\end{aligned}$$

respectively, where $v = (v^1, v^2) \in \mathbb{R}^{(N-1) \times M} \times \mathbb{R}^{N \times (M-1)}$. We note that different components of ∇u , Jv , $\mathcal{E}v$ have different length. Using these objects, we define discrete versions of TV, second order TV, of TV-TV² infimal convolution and of TGV as

$$\begin{aligned}\text{TV}(u) &= \|\nabla u\|_1, & \text{TV}^2(u) &= \|J\nabla u\|_1, & \text{IC}_\alpha(u) &= \min_v \alpha_1 \text{TV}(u - v) + \alpha_0 \text{TV}^2(v), \\ \text{TGV}_\alpha^2(u) &= \min_w \alpha_1 \|\nabla u - w\|_1 + \alpha_0 \|\mathcal{E}w\|_1.\end{aligned}\tag{12}$$

Here, $\|\cdot\|_1$ denotes the ℓ^1 norm w.r.t. the spatial component and we take an ℓ^p norm (with $p \in [1, \infty)$) in the vector components without explicit mentioning, e.g.,

$\|\nabla u\|_1 := \sum_{i,j} ((\delta_x u)_{i,j}^p + (\delta_y u)_{i,j}^p)^{1/p}$, where we again replace summands containing out-of-bound indices 0. Note that the most interesting cases are $p = 1$ due to advantages for the numerical realization and $p = 2$ since this corresponds to isotropic functionals in the infinite-dimensional vector-space case, see for instance [28] for TGV. Also note that $(J\nabla u)_{i,j}$ is symmetric, that the symmetric component of $\mathcal{E}w$ is stored only once and that we define $\|\mathcal{E}w\|_1 := \sum_{i,j} \left((\delta_x w^1)_{i,j}^p + (\delta_y w^2)_{i,j}^p + 2(\frac{\delta_y w^1 + \delta_x w^2}{2})_{i,j}^p \right)^{1/p}$ to compensate for that.

Now we extend these regularizers to arguments $u \in \mathcal{M}^{N \times M}$ with \mathcal{M} being a complete, finite dimensional Riemannian manifold with induced distance d . For the sake of highlighting the main ideas first, we start with the univariate situation $u = (u_i)_i \in \mathcal{M}^N$.

Regarding second order TV, following [9], we observe (with δ the univariate version of δ_x) that, for $u \in (\mathbb{R}^d)^N$ and a norm $\|\cdot\|$ on \mathbb{R}^d ,

$$\|(\delta \delta u)_i\| = \|u_{i+1} - 2u_i + u_{i-1}\| = 2\left\| \frac{u_{i+1} + u_{i-1}}{2} - u_i \right\|,$$

where the last expression only requires averaging and a distance measure, both of which is available on Riemannian manifolds. Thus, a generalization of TV² for $u \in \mathcal{M}^N$ can be given, for $u = (u_i)_i$, by

$$\text{TV}^2(u) = \sum_i D_c(u_{i-1}, u_i, u_{i+1}) \quad \text{where } D_c(u_-, u_o, u_+) = \inf_{c \in [u_-, u_+]_{\frac{1}{2}}} 2d(c, u_o).$$

Here, D_c essentially measures the distance between the central data point u_o and the geodesic midpoint of its neighbors, if this midpoint is unique, and the infimum w.r.t. all midpoints otherwise. Similarly, we observe for mixed derivatives and $u \in (\mathbb{R}^d)^{N \times N}$ that

$$\|(\delta_y \delta_x u)\| = 2 \left\| \frac{u_{i+1,j} + u_{i,j-1}}{2} - \frac{u_{i,j} + u_{i+1,j-1}}{2} \right\|.$$

An analogue for $u \in \mathcal{M}^{M \times M}$ is hence given by

$$D_{cc}(u_{i,j}, u_{i+1,j}, u_{i,j-1}, u_{i+1,j-1}) = \inf_{c_1 \in [u_{i+1,j}, u_{i,j-1}]_{\frac{1}{2}}, c_2 \in [u_{i,j}, u_{i+1,j-1}]_{\frac{1}{2}}} 2d(c_1, c_2),$$

and similarly for $\delta_x \delta_y$. Exploiting symmetry, we only incorporate $(\delta_y \delta_x u)$ and define

$$\begin{aligned} \text{TV}^2(u) = \sum_{i,j} & \left(D_c(u_{i-1,j}, u_{i,j}, u_{i+1,j})^p + D_c(u_{i,j-1}, u_{i,j}, u_{i,j+1})^p \right. \\ & \left. + 2D_{cc}(u_{i,j}, u_{i+1,j}, u_{i,j-1}, u_{i+1,j-1})^p \right)^{1/p}. \end{aligned}$$

This generalizes second order TV for manifold-valued data while still relying only on point-operations on the manifold. As will be shown in Section 3.2, numerical result for TV^2 denoising show less staircasing than TV denoising. However, it tends towards oversmoothing which is expected from the underlying theory and corresponding numerical results in the vector space case.

A possible extension of TV-TV² infimal-convolution to manifolds is based on a representation in the linear space case given as

$$\text{IC}_\alpha(u) = \inf_v \alpha_1 \text{TV}(u - v) + \alpha_0 \text{TV}^2(v) = (1/2) \inf_{v, w: u = \frac{v+w}{2}} \alpha_1 \text{TV}(v) + \alpha_0 \text{TV}^2(w),$$

where $u = (u_{i,j})_{i,j} \in (\mathbb{R}^d)^{N \times M}$. This representation was taken in [14, 15] and extended for $u = (u_{i,j})_{i,j} \in \mathcal{M}^{N \times M}$ (up to constants) via

$$\text{IC}(u) = \frac{1}{2} \inf_{v,w} \alpha_1 \text{TV}(v) + \alpha_0 \text{TV}^2(w) \quad \text{s.t. } u_{i,j} \in [[v_{i,j}, w_{i,j}]]_{\frac{1}{2}},$$

where $v = (v_{i,j})_{i,j}$ and $w = (w_{i,j})_{i,j}$. Following [14], we here use the symbol $[[v_{i,j}, w_{i,j}]]$ instead of $[v_{i,j}, w_{i,j}]$, where we define the former to include also non-distance minimizing geodesics.

In order to generalize the second order TGV functional to a manifold setting, we consider (12) for vector spaces. This definition (via optimal balancing) requires to measure the distance of (discrete) vector fields that are in general defined in different tangent spaces. One means to do so is to employ parallel transport for vector fields in order to shift different vector fields to the same tangent space and to measure the distance there. (We note that the particular locations the vectors are shifted to is irrelevant since the values are equal.) This approach requires to incorporate more advanced concepts on manifolds. Another possibility is to consider a *discrete tangent space* of point tuples via the identification of $v = \log_a(b)$ as a point tuple $[a, b]$ (where \log is the inverse exponential map), and to define a distance-type function on such point tuples. Indeed, the above identification is one-to-one except for points on the cut locus (which is a set of measure zero [67]) and allows to identify discrete derivatives $(\delta_x u)_i = (u_{i+1} - u_i) = \log_{u_i}(u_{i+1})$ as tuple $[u_i, u_{i+1}]$. Choosing appropriate distance type functions, this identification allows to work exclusively on the level of point-operations and one might say that the “level of complexity” of the latter approach is comparable with that of TV^2 and IC. Furthermore, a version of the above parallel transport variant can be realized in the tuple setting as well (still incorporating more

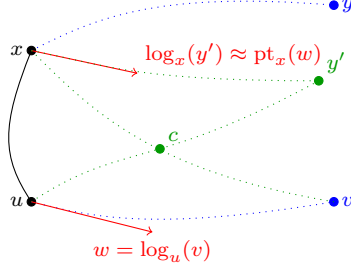


Figure 5: Approximate parallel transport of $\log_u(v)$ to x via the Schild's ladder construction. Figure taken from [27].

advanced concepts). This approach was proposed in [27]; more precisely, an axiomatic approach is pursued in [27] and realizations via Schild's ladder (requiring only point operations) and parallel transport are proposed and shown to be particular instances of the axiomatic approach.

We explain the approach in more detail, where we focus on the univariate situation first. We assume for the moment that $D : \mathcal{M}^2 \times \mathcal{M}^2$ is an appropriate distance-type function for point tuples. Then, a definition of TGV_α^2 for an univariate signal $u = (u_i)_i \in \mathcal{M}^N$ can be given as

$$\text{TGV}_\alpha^2((u_i)_i) = \inf_{(y_i)_i} \sum_i \alpha_1 D([u_i, u_{i+1}], [u_i, y_i]) + \alpha_0 D([u_i, y_i], [u_{i-1}, y_{i-1}]).$$

Thus, one is left to determine a suitable choice of D . One possible choice is based on the Schild's ladder [72] approximation of parallel transport, which is defined as follows (see Figure 5): Assuming, for the moment, uniqueness of geodesics, define $c = [v, x]_{\frac{1}{2}}$ and $y' = [u, c]_2$. Then $[x, y']$ can be regarded as approximation of the parallel transport of $w = \log_u(v)$ to x , which is exact in the vector-space case. Motivated by this, the distance of the tuples $[u, v]$ and $[x, y]$ can be defined as $d(y, y')$. Incorporating non-uniqueness by minimizing over all possible points in this construction to capture also points on the cut locus, yields a distance-type function for point tuples given as

$$D_S([x, y], [u, v]) = \inf_{y' \in \mathcal{M}} d(y, y') \quad \text{s.t. } y' \in [u, c]_2 \text{ with } c \in [x, v]_{\frac{1}{2}}.$$

In the particular case that both tuples have the same base point, i.e., $x = u$, it is easy to see that, except in the case of non-unique length-minimizing geodesics, $D_S([x, y], [x, v]) = d(v, y)$ such that we can use this as simplification and arrive at a concrete form of manifold-TGV for univariate signals $(u_i)_i$ in \mathcal{M} given as

$$\text{S-TGV}_\alpha^2((u_i)_i) = \inf_{(y_i)_i} \sum_i \alpha_1 d(u_{i+1}, y_i) + \alpha_0 D_S([u_i, y_i], [u_{i-1}, y_{i-1}]).$$

We note that this operation only requires to carry out averaging and reflection followed by applying the distance in the manifold. Thus it is on the same “level of difficulty” as TV^2 or IC. For the bivariate situation, the situation is more challenging due to an additional averaging involved in the evaluation of $\mathcal{E}w$. In fact, as described in [27], there are different possibilities (of varying complexity) to generalize this to the manifold valued setting but there is a unique, rather simple one which in addition transfers fundamental properties of TGV, such as a precise knowledge on its kernel, to the manifold setting. This leads to the definition of $D_S^{\text{sym}} : (\mathcal{M}^2)^4$ which realizes the symmetrized part of $\mathcal{E}w$ in the definition of TGV and for which, for the

sake of brevity, we refer to [27, Equation 20]. Using D_S^{sym} , a bivariate version of TGV for $u = (u_{i,j})_{i,j} \in \mathcal{M}^{N \times M}$ is given as

$$\begin{aligned} \text{S-TGV}_\alpha^2(u) &= \min_{y_{i,j}^1, y_{i,j}^2} \alpha_1 \sum_{i,j} \left(d(u_{i+1,j}, y_{i,j}^1)^p + d(u_{i,j+1}, y_{i,j}^2)^p \right)^{1/p} \\ &+ \alpha_0 \sum_{i,j} \left(D_S([u_{i,j}, y_{i,j}^1], [u_{i-1,j}, y_{i-1,j}^1])^p + D_S([u_{i,j}, y_{i,j}^2], [u_{i,j-1}, y_{i,j-1}^2])^p \right. \\ &\left. + 2^{1-p} D_S^{\text{sym}}([u_{i,j}, y_{i,j}^1], [u_{i,j}, y_{i,j}^2], [u_{i,j-1}, y_{i,j-1}^1], [u_{i-1,j}, y_{i-1,j}^2])^p \right)^{1/p}. \end{aligned} \quad (13)$$

Naturally, the above definition of S-TGV based on the Schild's ladder construction is not the only possibility to extend second order TGV to the manifold setting. As already pointed out, in [27] this was accounted for by an axiomatic approach which, for a suitable generalization, also requires additional properties such as a good description of their kernel, and we will see below that indeed this is possible for S-TGV. An alternative definition based on parallel transport presented in [27] uses, instead of D_S for point-tuples with different base points, the distance

$$D_{\text{pt}}([x, y], [u, v]) = \|\log_x(y) - \text{pt}_x(\log_u(v))\|_x, \quad (14)$$

where $\text{pt}_x(z)$ is the parallel transport of $z \in T\mathcal{M}$ to $T_x\mathcal{M}$, and a similar adaption of D_S^{sym} for bivariate signals. It was shown in [27] that also this version suitably generalizes TGV by transferring some of its main properties to the manifold setting.

Another existing extension of TGV to the manifold setting is the one presented in [15] which is given, in the univariate setting, as

$$\widetilde{\text{TGV}}_\alpha^2(u) = \inf_{(\xi_i)_i} \sum_i \alpha_1 \|\log_{u_i}(u_{i+1}) - \xi_i\|_{u_i} + \alpha_0 \|\xi_i - P_{u_i}(\xi_{i-1})\|_{u_i}$$

where P_{u_i} approximates the parallel transport of ξ_{i-1} to u_i by first mapping it down to a point tuple $[u_{i-1}, \exp_{u_{i-1}}(\xi_i)]$, then using the pole ladder [75] as an alternative to Schild's ladder to approximate the parallel transport to u_i and finally lifting the transported tuple again to the tangent space via the logarithmic map. In the univariate case, this also generalizes TGV and preserves its main properties such as a well defined kernel. For the bivariate version, [15] uses the standard Jacobian instead of the symmetrized derivative and it remains open to what extend the kernel of TGV is appropriately generalized, also because there is no direct, natural generalization of the kernel of TGV_α^2 (i.e., affine functions) in the bivariate setting (see the next paragraph for details).

Consistency. Given that there are multiple possibilities of extending vector-space concepts to manifolds, the question arises to what extend the extensions of TV^2 , IC and TGV presented above are natural or “the correct ones.” As observed in [27], the requirement of suitably transferring the kernel of the vector-space version, which consists of the set of affine functions, is a property that at least allows to reduce the number of possible generalizations. Motivated by this, we consider the zero-set of the manifold extensions of TV^2 , IC_α and TGV_α^2 . We start with the univariate situation, where a generalization of the notion of “affine” is rather natural.

Definition 2 (Univariate generalization of affine signals). *Let $u = (u_i)_i$ be a signal in \mathcal{M}^N . We say that u is generalized affine or geodesic if there exists a geodesic $\gamma : [0, L] \rightarrow \mathcal{M}$ such that all points of u are on γ at equal distance and γ is length-minimizing between two subsequent points.*

The following proposition relates geodesic functions to the kernel of higher-order regularizers on manifolds. Here, in order to avoid ambiguities arising from subtle difference in the functionals

depending on if length-minimizing geodesics are used or not, we assume geodesics are unique noting that the general situation is mostly analogue.

Proposition 3 (Consistency, univariate). *Let $u = (u_i)_i$ in \mathcal{M} be such that all points u_i, u_j are connected by a unique geodesic.*

(i) *If u is geodesic, $\text{TV}^2(u) = \text{IC}_\alpha(u) = \text{S-TGV}_\alpha^2(u) = 0$.*

(ii) *Conversely, if $\text{TV}^2(u) = 0$ or $\text{S-TGV}_\alpha^2(u) = 0$, then u is geodesic.*

Proof. If u is geodesic, it follows that $u_i \in [u_{i-1}, u_{i+1}]_{\frac{1}{2}}$, such that $\text{TV}^2(u) = 0$. In case of IC_α define $v_i = u_1$ (the first point of u) for all i and $w_i = [u_1, u_i]_{2d(u_1, u_i)}$. Then it follows that $u_i \in [v_i, w_i]_{\frac{1}{2}}$ for all i . Further, $\text{TV}((v_i)_i) = 0$ and, since $(w_i)_i$ is geodesic, also $\text{TV}^2((w_i)_i) = 0$ such that $\text{IC}_\alpha(u) = 0$. Regarding S-TGV_α^2 , we see that $\text{S-TGV}_\alpha^2(u) = 0$ follows from choosing $(y_i)_i = (u_{i+1})_i$ and noting that $D_S([u_i, u_{i+1}], [u_{i-1}, u_i]) = 0$ since $u_i \in [u_i, u_i]_{\frac{1}{2}}$ and $u_{i+1} \in [u_{i-1}, u_i]_2$. Now conversely, if $\text{TV}^2(u) = 0$, it follows that $u_i \in [u_{i-1}, u_{i+1}]$ for all i such that $(u_i)_i$ is geodesic. If $\text{S-TGV}_\alpha^2(u) = 0$ we obtain $(y_i)_i = (u_{i+1})_i$ and, consequently, $u_{i+1} \in [u_i, u_{i-1}]$ which again implies that u is geodesic. \square

Remark 4. *One can observe that in Proposition 3, the counterparts of ii) for IC_α is missing. Indeed, an easy counterexample shows that this assertion is not true, even in case of unique geodesics: Consider $\mathcal{M} = \mathcal{S}^2 \cap ([0, \infty) \times \mathbb{R} \times [0, \infty))$ and $\phi_1 = -\pi/4, \phi_2 = 0, \phi_3 = \pi/4$ and $\psi = \pi/4$ define*

$$\begin{aligned} u_i &= (\cos(\varphi_i) \sin(\psi), \sin(\varphi_i) \sin(\psi), \cos(\psi)) \\ w_i &= (\cos(\varphi_i), \sin(\varphi_i), 0) \end{aligned}$$

and $v_i = (0, 0, 1)$ for all i . Then $u_i \in [v_i, w_i]_{\frac{1}{2}}$, $\text{TV}(v) = 0$, $\text{TV}^2(w) = 0$, hence $\text{IC}_\alpha(u) = 0$ but u is not geodesic.

In the bivariate setting, a generalization of an affine function is less obvious: It seems natural that $u = (u_{i,j})_{i,j}$ being *generalized affine* or, in the notion above, *geodesic* should imply that for each k , both $(u_{i,k})_i$ and $(u_{k,j})_j$ are geodesics. However, to achieve a generalization of affine, an additional condition is necessary to avoid functions of the form $(x, y) \mapsto xy$. In [27] this condition was to require also the signal $(u_{i+k, j-k})_k$ to be geodesic for each i, j . While this has the disadvantage favoring one particular direction, it is less restrictive than to require, in addition, also $(u_{i+k, j+k})_k$ to be geodesic. As shown in the following proposition, bivariate functions that are geodesic in the sense of [27] coincide with the kernel of S-TGV_α^2 . TV^2 on the other hand, gives rise to a different notion of affine.

Proposition 5 (Kernel, bivariate). *Let $u = (u_{i,j})_{i,j}$ be such that all points of u are connected by a unique geodesics.*

(i) *$\text{S-TGV}_\alpha^2(u) = 0$ if and only if $(u_{k,j_0})_k$, $(u_{i_0,k})_k$ and $(u_{i_0+k, j_0-k})_k$ is geodesic for each i_0, j_0 .*

(ii) *$\text{TV}^2(u) = 0$ if and only if $(u_{k,j_0})_k$, $(u_{i_0,k})_k$ is geodesic for each i_0, j_0 and $[u_{i+1,j}, u_{i,j-1}]_{\frac{1}{2}} \cap [u_{i,j}, u_{i+1,j-1}]_{\frac{1}{2}} \neq \emptyset$ for all i, j .*

Proof. For S-TGV_α^2 , a stronger version of this result is proven in [27, Theorem 2.18]. For TV^2 , this follows analogously to the univariate case directly from the definition of D_c and D_{cc} . \square

Higher-order regularized denoising. The next proposition shows that TV^2 and S-TGV based denoising of manifold valued data is indeed well-posed.

Proposition 6. *Both TV^2 and S-TGV_α^2 are lower semi-continuous w.r.t. convergence in (\mathcal{M}, d) . Further, for $R \in \{\alpha \text{TV}^2, \text{S-TGV}_\alpha^2\}$, where $\alpha > 0$ the the case of TV^2 , the problem*

$$\inf_{u=(u_{i,j})_{i,j}} R(u) + \sum_{i,j} d(u_{i,j}, f_{i,j})^q$$

admits a solution.

Proof. The proof is quite standard: by the Hopf-Rinow theorem, it is clear that the claimed existence follows once lower semi-continuity of R can be guaranteed. For S-TGV_α^2 , this is the assertion of [27, Theorem 3.1]. For TV^2 , it suffices to show lower semi-continuity of D_c and D_{cc} . We provide a proof for D_c , the other case works analogously. Take $u^n = (u_-^n, u_\circ^n, u_+^n)_n$ converging to (u_-, u_\circ, u_+) and take $(c_n)_n$ with $c_n \in [u_-^n, u_+^n]$ such that $d(c_n, u_\circ^n) \leq \inf_{c \in [u_-^n, u_+^n]} d(c, u_\circ^n) + 1/n$. Then, from boundedness of $(u^n)_n$ and since $d(c^n, u_-^n) \leq d(u_+^n, u_-^n)$ we obtain boundedness of $(c^n)_n$, hence a (non-relabelled) subsequence converging to some $c \in \mathcal{M}$ exists. From uniform convergence of the geodesics $\gamma^n : [0, 1] \rightarrow \mathcal{M}$ connecting u_-^n and u_+^n such that $c^n = \gamma^n(1/2)$ (see for instance [27, Lemma 3.3]) we obtain that $c \in [u_-, u_+]_{\frac{1}{2}}$ such that $D_c(u_-, u_\circ, u_+) \leq d(c, u_\circ) \leq \liminf_n d(c_n, u_\circ^n) \leq \liminf_n D_c(u_-^n, u_\circ^n, u_+^n)$. \square

Remark 7. *We note that the arguments of Proposition 6 do not apply to IC since we cannot expect $(v_{i,j})_{i,j}$ and $(w_{i,j})_{i,j}$ with $u_{i,j} \in [v_{i,j}, w_{i,j}]_{\frac{1}{2}}$ to be bounded in general. Indeed, this is similar to vector-space infimal convolution, only that there, one can factor out the kernel of TV and still obtain existence.*

3.2 Algorithmic Realization

Here we discuss the algorithmic realization and illustrate the results of TV^2 and S-TGV regularized denoising; for IC we refer to [14, 15]. We note that, in contrast to the TV functional, the TV^2 and the S-TGV_α^2 functional are not convex on Hadamard manifolds (cf. [9, Remark 4.6]) such that we cannot expect to obtain numerical algorithms that provably converge to global optimal solutions as for TV in Hadamard spaces (cf. Theorem 1). Nevertheless, the cyclic proximal point algorithm and the parallel proximal point algorithm as described in Section 2.2 are applicable in practice. In the following, we discuss the corresponding splittings and proximal mappings, where we focus on the univariate case since, similar to Section 2.2, the bivariate case for $p = 1$ can be handled analogously; for details we refer to [9, 27].

For TV^2 denoising, we may use the splitting

$$\frac{1}{q} \sum_i d(u_i, f_i)^q + \alpha \text{TV}^2((u_i)_i) = F_0(u) + F_1(u) + F_2(u) + F_3(u)$$

where $F_0(u) = \frac{1}{q} \sum_i d(u_i, f_i)^q$, and

$$F_j(u) = \sum_i D_c(u_{3i-1+j}, u_{3i+j}, u_{3i+1+j}), \quad j = 1, \dots, 3.$$

Due to the decoupling of the summands, the computation of the proximal maps of $(F_i)_{i=0}^3$ reduces to the computation of the proximal maps of $x \mapsto d(x, f)^q$ and of $(x_1, x_2, x_3) \mapsto D_c(x_1, x_2, x_3)$. The former is given explicitly as in (8), while for the latter, following [9], we use a subgradient descent scheme (see for instance [47]) to iteratively solve

$$\min_{x_{k-1}, x_k, x_{k+1}} \frac{1}{2} \sum_{l=k-1}^{k+1} d^2(x_l, h_l) + \lambda D_c(x_{k-1}, x_k, x_{k+1})$$

Algorithm 3 Subgradient descent for solving $\min_x F(x)$

```

1: SGD( $x_0, (\lambda_i)_i$ )
2:  $l = 0$ 
3:   repeat until stopping criterion fulfilled
4:      $x_{k+1} \leftarrow \exp_{x_k}(-\lambda_k \partial F(x_k))$ 
5:      $k \leftarrow k + 1$ 
6: return  $x$ 

```

for $(h_{k-1}, h_k, h_{k+1}) \in \mathcal{M}^3$ the given point where the proximal map needs to be computed.

For this purpose, we employ Algorithm 3, which requires to compute the subgradient of D_c as well as the derivative of d . The latter is, at a point (x_{k-1}, x_k, x_{k+1}) given as

$-(\log_{x_{k-1}}(h_{k-1}), \log_{x_k}(h_k), \log_{x_{k+1}}(h_{k+1}))^T$. Regarding the computation of D_c , in order to avoid pathological (and practically irrelevant) constellations, we assume that the arguments x_{k-1}, x_{k+1} are not cut points, such that there is exactly one length minimizing geodesics connecting x_{k-1} and x_{k+1} and the corresponding midpoint is unique. With these assumptions, the derivative w.r.t. the first component and for a point (x, y, z) with $y \neq [x, z]_{\frac{1}{2}}$ is given as

$$\partial_y D_c(x, \cdot, z)(y) = \log_y([x, z]_{\frac{1}{2}}) / \|\log_y([x, z]_{\frac{1}{2}})\|_y.$$

The derivative w.r.t. x is given by

$$\partial_x D_c(\cdot, y, z)(x) = \sum_{l=1}^d \langle \log_c(y) / \|\log_c(y)\|_c, D_x c(\xi_l) \rangle$$

where we denote $c = [x, z]_{\frac{1}{2}}$. Here, $D_x c$ is the differential of the mapping $c : x \mapsto [x, z]_{\frac{1}{2}}$ which is evaluated w.r.t. the elements of an orthonormal basis $(\xi_l)_{l=1}^d$ of the tangent space at x . The derivative w.r.t. z is computed analogously due to symmetry and for the particular case that $y = [x, z]_{\frac{1}{2}}$ we refer to [9, Remark 3.4]. While the formulas above provide general forms of the required derivatives, a concrete realization can be done using explicit formulae for Jacobi fields in the particular manifold under consideration; we refer to [9] for explicit versions. For the bivariate case, we also refer to [9] for the derivative of D_{cc} , which can be computed with similar techniques as D_c .

For TGV, we again start with the univariate case and consider the S-TGV_α^2 variant. We consider the splitting

$$\frac{1}{q} \sum_i d(u_i, f_i)^q + \text{TGV}_\alpha^2((u_i)_i) = F_0(u) + F_1(u) + F_2(u) + F_3(u)$$

where $F_0(u) = \frac{1}{q} \sum_i d(u_i, f_i)^q$, $F_1(u) = \sum_i d(u_{i+1}, y_i)$, and

$$F_2(u) = \sum_{i:i \text{ even}} D_S([u_i, y_i], [u_{i-1}, y_{i-1}]), \quad F_3(u) = \sum_{i:i \text{ odd}} D_S([u_i, y_i], [u_{i-1}, y_{i-1}]).$$

Here, as an advantage of this particular version of TGV that uses only points on the manifold, we see that the proximal mappings of F_1 are explicit as in (10) and, since again the proximal mapping of F_0 is given for $q \in \{1, 2\}$ explicitly by (8), we are left to compute the proximal mappings for D_S . To this aim, we again apply the subgradient descent method as in Algorithm 3, where the required derivatives of D_S are provided in [27]. In particular, again assuming uniqueness of geodesics to avoid pathological situations, we have that for points $[u_i, y_i], [u_{i-1}, y_{i-1}]$ with $y_i \neq [u_{i-1}, [u_i, y_{i-1}]_{\frac{1}{2}}]_2$ that

$$\nabla_{y_i} D_S = -\log_{y_i} S(u_{i-1}, y_{i-1}, u_i) / \|\log_{y_i} S(u_{i-1}, y_{i-1}, u_i)\| \quad (15)$$

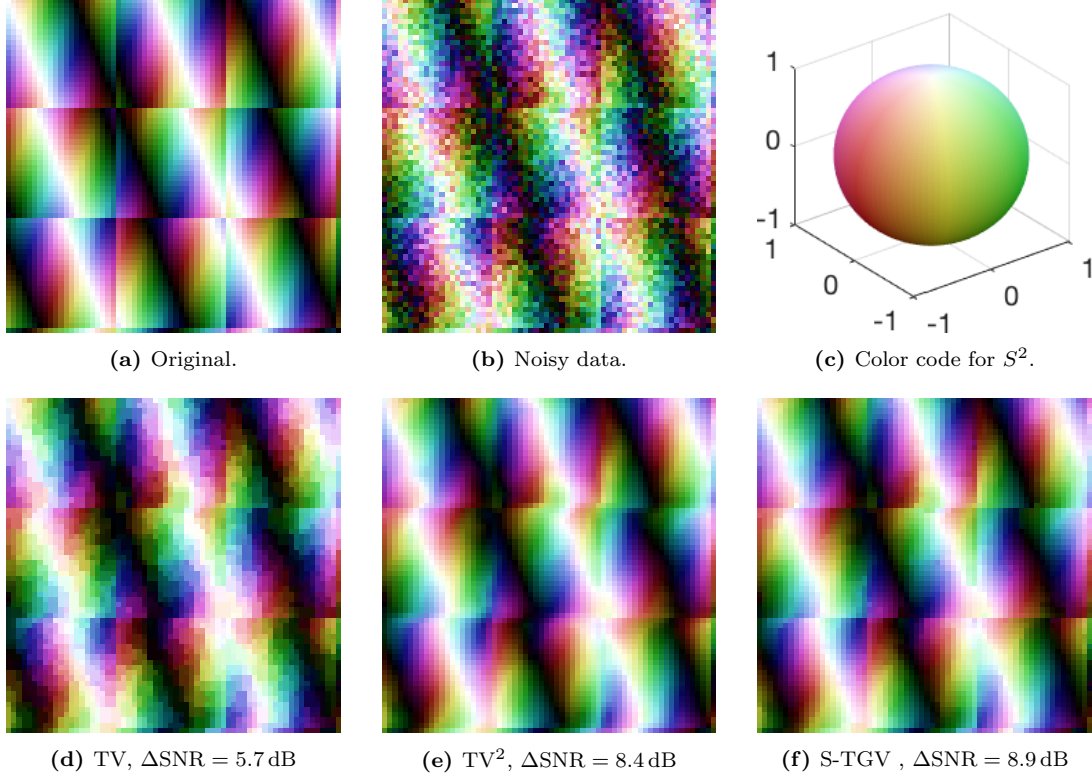


Figure 6: Comparison of first and second-order total variation as well as S-TGV on an S^2 -valued image from [9]. Images taken from [27].

where

$$S(u_{i-1}, y_{i-1}, u_i) = [u_{i-1}, [u_i, y_{i-1}]_{1/2}]_2 \quad (16)$$

denotes the result of applying the Schild's construction to the respective arguments. Derivatives w.r.t. the arguments u_{i-1} and y_{i-1} are given in abstract form as

$$\nabla_{u_{i-1}} D_S = -T_1 \left(\log_{S(u_{i-1}, y_{i-1}, u_i)} y_i / \left\| \log_{S(u_{i-1}, y_{i-1}, u_i)} y_i \right\| \right), \quad (17)$$

$$\nabla_{y_{i-1}} D_S = -T_2 \left(\log_{S(u_{i-1}, y_{i-1}, u_i)} y_i / \left\| \log_{S(u_{i-1}, y_{i-1}, u_i)} y_i \right\| \right), \quad (18)$$

where T_1 is the adjoint of the differential of the mapping $u_{i-1} \mapsto [u_{i-1}, [u_i, y_{i-1}]_{1/2}]_2$, and T_2 is the adjoint of the differential of the mapping $y_{i-1} \mapsto [u_{i-1}, [u_i, y_{i-1}]_{1/2}]_2$. The differential w.r.t. u_i is obtained by symmetry. Again, the concrete form of these mappings depends on the underlying manifold and we refer to [27] for details. Regarding points with $y_i \neq [u_{i-1}, [u_i, y_{i-1}]_{1/2}]_2$ we note that for instance the four-tuple consisting of the four zero-tangent vectors sitting in $u_i, u_{i-1}, [u_{i-1}, [u_i, y_{i-1}]_{1/2}]_2, y_{i-1}$ belongs to the subgradient of D_S . The algorithm for bivariate TGV-denoising can be obtained analogously, where we refer to [27] for the computation of the derivative of D_S^{sym} . The algorithm for TGV-denoising based on the parallel variant (14) employs the proximal mappings of F_0 and F_1 as well. Implementation of the proximal mappings of F_2 and F_3 based on subgradient descent can be found in [27] and [26].

Numerical examples. We illustrate the algorithm with numerical examples. At first, we

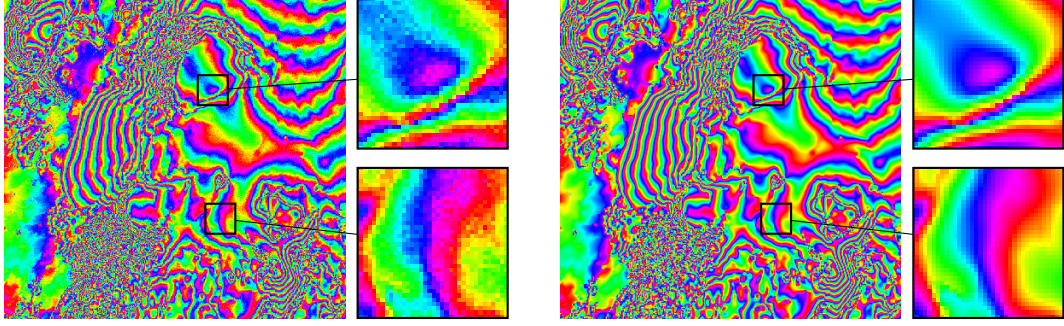


Figure 7: *Left:* InSAR image from [102]. *Right:* Result of S-TGV. Image taken from [27].

provide a comparison between TV, TV^2 and S-TGV regularization for synthetic S^2 -valued image data, taken from [27]. The results can be found in Figure 6, where for each approach we optimized over the involved parameters to achieve the best ΔSNR result, with ΔSNR being defined for ground truth, noisy and denoised signals h , f and u , respectively, as $\Delta SNR = 10 \log_{10} \left(\frac{\sum_i d(h_i, f_i)^2}{\sum_i d(h_i, u_i)^2} \right)$ dB. We observe that the TV regularization produces significant piecewise constancy artifacts (staircasing) on the piecewise smooth example. The result of TV^2 shows no visible staircasing, but smoothes the discontinuities to some extent. S-TGV is able to better reconstruct sharp interfaces while showing no visible staircasing.

As second example, Figure 7 considers the denoising of interferometric synthetic aperture radar (InSAR) images. Again, it can be observed that S-TGV has a significant denoising effect while still preserving sharp interfaces.

4 Mumford-Shah Regularization for Manifold Valued Data

The Mumford and Shah model [79, 80], also called Blake-Zisserman model [20], is a powerful variational model for image regularization. The regularization term measures the length of the jump set and, within segments, it measures quadratic variation of the function. The resulting regularization is a smooth approximation to the image/signal which, at the same time, allows for sharp edges at the discontinuity set. Compared with the TV regularizer, it does not penalize the jump height and, due to the quadratic variation on the complement of the edge set, no staircasing effects appear. (Please note that no higher order derivatives/differences are involved here.) The piecewise constant variant of the Mumford-Shah model (often called Potts model) considers piecewise constant functions (which then have no variation on the segments) and penalizes the length of the jump sets. Typical applications of these functionals are smoothing and the use within a segmentation pipeline. For further information considering these problems for scalar data from various perspectives (calculus of variation, stochastics, inverse problems) we refer to [85, 20, 54, 4, 30, 120, 23, 52, 51, 68] and the references therein. These references also deal with fundamental questions such as the existence of minimizers. Mumford-Shah and Potts problems are computationally challenging since the functionals are non-smooth and non-convex. Even for scalar data, both problems are known to be NP-hard in dimensions higher than one [106, 22, 2]. This makes finding a (global) minimizer infeasible. Because of its importance in image processing however, many approximative strategies have been proposed for scalar- and vector valued data. Among these strategies are graduated non-convexity [20], approximation by elliptic functionals [4], graph cuts [22], active contours [104], convex relaxations [84], iterative

thresholding approaches [52], and alternating direction methods of multipliers [66].

In the context of DTI, the authors of [112, 111] consider a Chan-Vese model for positive matrix-valued data, i.e., for manifold-valued data in Pos_3 , as well as a piecewise smooth variant. (We recall that Chan-Vese models are variants of Potts models for the case of two labels.) Their method is based on a level-set active-contour approach. In order to reduce the computational load in their algorithms (which is due to the computation of Riemannian means for a very large number of points) the authors resort to non-Riemannian distance measures in [112, 111]. Recently, a fast recursive strategy for computing the Riemannian mean has been proposed and applied to the piecewise constant Chan-Vese model (with two labels) in [38].

We mention that for \mathbb{S}^1 -valued data, a noniterative exact solver for the univariate Potts problem has been proposed in [99].

In this section, we consider Mumford-Shah and Potts problems for (general) manifold-valued data and derive algorithms for these problems. As in the linear case, typical applications of these functionals are smoothing and also segmentation; more precisely, they can serve as an initial step of a segmentation pipeline. In simple cases, the induced edge set may yield a reasonable segmentation directly.

4.1 Models

We start out with Mumford-Shah and Potts problems for univariate manifold-valued data $(f_i)_{i=1}^N \in \mathcal{M}^N$, with \mathcal{M} again being a complete, finite dimensional Riemannian manifold. The discrete Mumford-Shah functional reads

$$B_{\alpha,\gamma}(x) = \frac{1}{q} \sum_{i=1}^N d(x_i, f_i)^q + \frac{\alpha}{p} \sum_{i \notin \mathcal{J}(x)} d(x_i, x_{i+1})^p + \gamma |\mathcal{J}(x)|, \quad (19)$$

where d is the distance with respect to the Riemannian metric in the manifold \mathcal{M} , \mathcal{J} is the jump set of x and $p, q \in [1, \infty)$. The jump set is given by $\mathcal{J}(x) = \{i : 1 \leq i < n \text{ and } d(x_i, x_{i+1}) > s\}$, and $|\mathcal{J}(x)|$ denotes the number of jumps. The jump height s and the parameter γ are related via $\gamma = \alpha s^p / p$. We rewrite (19) using a truncated power function to obtain the Blake-Zisserman type form

$$B_{\alpha,s}(x) = \frac{1}{q} \sum_{i=1}^N d(x_i, f_i)^q + \frac{\alpha}{p} \sum_{i=1}^{N-1} \min(s^p, d(x_i, x_{i+1})^p), \quad (20)$$

where s is the argument of the power function $t \mapsto t^p$, which is truncated at $d(x_i, x_{i+1})^p$. The discrete univariate Potts functional for manifold-valued data reads

$$P_\gamma(x) = \frac{1}{q} \sum_{i=1}^n d(x_i, f_i)^q + \gamma |\mathcal{J}(x)|, \quad (21)$$

where an index i belongs to the jump set of x if $x_i \neq x_{i+1}$.

In the multivariate situation, the discretization of the Mumford-Shah and Potts problem is not as straightforward as in the univariate case. A simple finite difference discretization with respect to the coordinate directions is known to produce undesired block artifacts in the reconstruction [31]. The results improve significantly when including further finite differences such as the diagonal directions [31, 93, 97]. To define bivariate Mumford-Shah and Potts functionals, we introduce the notation $d^q(x, y) = \sum_{i,j} d^q(x_{ij}, y_{ij})$ for the q -distance of two manifold-valued images $x, y \in \mathcal{M}^{N \times M}$. For the regularizing term, we employ the penalty function

$$\Psi_a(x) = \sum_{i,j} \psi(x_{(i,j)+a}, x_{ij}),$$

where $a \in \mathbb{Z}^2 \setminus \{0\}$ denotes a direction, and the potentials ψ are given by

$$\psi(w, z) = \frac{1}{p} \min(s^p, d(w, z)^p), \quad \text{and} \quad \psi(w, z) = \begin{cases} 1, & \text{if } w \neq z, \\ 0, & \text{if } w = z, \end{cases} \quad (22)$$

for $w, z \in \mathcal{M}$, in the Mumford-Shah case and in the Potts case, respectively. We define the discrete multivariate Mumford-Shah and Potts problems by

$$\min_{x \in \mathcal{M}^{N \times M}} \frac{1}{q} d^q(x, f) + \alpha \sum_{s=1}^R \omega_s \Psi_{a_s}(x), \quad (23)$$

where the finite difference vectors $a_s \in \mathbb{Z}^2 \setminus \{0\}$ belong to a neighborhood system \mathcal{N} and $\omega_1, \dots, \omega_R$ are non-negative weights. As observed in [93], a reasonable neighborhood system is

$$\mathcal{N} = \{(1, 0); (0, 1); (1, 1); (1, -1)\}$$

with the weights $\omega_1 = \omega_2 = \sqrt{2} - 1$ and $\omega_3 = \omega_4 = 1 - \frac{\sqrt{2}}{2}$ as in [93]. It provides a sufficiently isotropic discretization while keeping the computational load at a reasonable level. For further neighborhood systems and weights we refer to [31, 93].

For both, the univariate and multivariate discrete Mumford-Shah and Potts functionals, the following result regarding the existence of minimizers holds.

Theorem 8. *Let \mathcal{M} be a complete Riemannian manifold. Then the univariate and multivariate discrete Mumford-Shah and Potts problems (19), (21), and (23) have a minimizer.*

A proof may be found in [117]. We note that most of the data spaces in applications are complete Riemannian manifolds.

4.2 Algorithmic Realization

We start with the univariate Mumford-Shah and Potts problems (19) and (21). These are not only important on their own, variants also appear as subproblems in the algorithms for the multivariate problems discussed below.

Dynamic programming scheme. To find a minimizer of the Mumford-Shah problem (19) and the Potts problem (21), we employ a general dynamic programming scheme which was employed for related scalar and vectorial problems in various contexts [80, 30, 119, 53, 118, 96]. We briefly explain the idea where we use the Mumford-Shah problem as example. We assume that we have already computed minimizers x^l of the functional $B_{\alpha, \gamma}$ associated with the partial data $f_{1:l} = (f_1, \dots, f_l)$ for each $l = 1, \dots, r-1$ and some $r \leq N$. (Here, we use the notation $f_{l:r} := (f_l, \dots, f_r)$.) We explain how to compute a minimizer x^r associated to data $f_{1:r}$. For each x^{l-1} of length $l-1$, we define a candidate $x^{l,r} = (x^{l-1}, h^{l,r}) \in \mathcal{M}^r$ which is the concatenation of x^{l-1} with a vector $h^{l,r}$ of length $r-l+1$; We choose $h^{l,r}$ as a minimizer of the problem

$$\epsilon_{l,r} = \min_{h \in \mathcal{M}^{r-l+1}} \sum_{i=l}^{r-1} \frac{\alpha}{p} d^p(h_i, h_{i+1}) + \frac{1}{q} \sum_{i=l}^r d^q(h_i, f_i), \quad (24)$$

where $\epsilon_{l,r}$ is the best approximation error on the (discrete) interval (l, \dots, r) . Then we calculate

$$\min_{l=1, \dots, r} \{B_{\alpha, \gamma}(x^{l-1}) + \gamma + \epsilon_{l,r}\}, \quad (25)$$

which coincides with the minimal functional value of $B_{\alpha, \gamma}$ for data $f_{1:r}$. We obtain the corresponding minimizer $x^r = x^{l^*, r}$, where l^* is a minimizing argument in (25). We successively

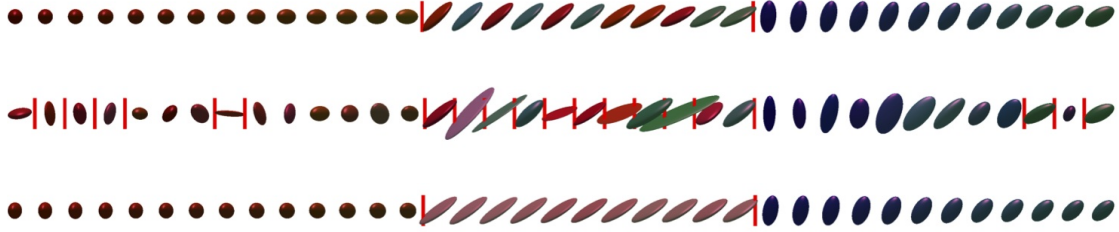


Figure 8: Univariate Mumford-Shah regularization ($p, q = 1$) using dynamic programming. (The red steaks indicate jumps.) *Top.* Original signal. *Middle.* Data with Rician noise added. *Bottom.* Regularized signal. Mumford-Shah regularization removes the noise while preserving the jump.

compute x^r for each $r = 1, \dots, N$ until we end up with full data f . For the selection process, only the l^* and the $\epsilon_{l,r}$ have to be computed; the optimal vectors x^r are then computed in a postprocessing step from these data; see, e.g., [53] for further details. This skeleton (without computing the $\epsilon_{l,r}$) has quadratic complexity with respect to time and linear complexity with respect to space. In the concrete situation, it is thus important to find fast ways for computing the approximation errors $\epsilon_{l,r}$. We will discuss this in the next paragraph for our particular situation. In practice, the computation is accelerated significantly using pruning strategies [73, 93].

Algorithms for the univariate Mumford-Shah and Potts problem. To make the dynamic program work for the Mumford-Shah problem with manifold-valued data, we have to compute the approximation errors $\epsilon_{l,r}$ in (24). These are L^q - V^p type problems: the data term is a manifold ℓ^q distance and the second term is a p th variation; in particular, for $p = 1$ we obtain TV minimization problems. These L^q - V^p problems can be solved using the proximal point schemes discussed in Section 2.1; for details, we refer to [116] where in particular the corresponding proximal mappings are calculated in terms of geodesic averages for the important case of quadratic variation $p = 2$.

To make the dynamic program work for the Potts problem with manifold-valued data, we have to compute the approximation errors $\epsilon_{l,r}$ for the problem $\epsilon_{l,r} = \min_{h \in \mathcal{M}^{r-l+1}} \frac{1}{q} \sum_{i=l}^r d^q(h_i, f_i)$, under the assumption that h is a constant vector. Hence we have to compute

$$\epsilon_{l,r} = \min_{h \in \mathcal{M}} \frac{1}{q} \sum_{i=l}^r d^q(h, f_i). \quad (26)$$

We observe that, by definition, a minimizer of (26) is given by an intrinsic mean for $q = 2$, and by an intrinsic median for $q = 1$, respectively.

As already discussed, a mean is general not uniquely defined since the minimization problem has no unique solution in general. Further, there is no closed form expression in general. One means to compute the intrinsic mean is the gradient descent (already mentioned in [70]) via the iteration

$$h^{k+1} = \exp_{h^k} \sum_{i=l}^r \frac{1}{r-l+1} \log_{h^k} f_i, \quad (27)$$

where again \log denotes the inverse exponential map. Further information on convergence and other related topics can for instance be found in the papers [50, 1] and the references given there. Newton's method was also applied to this problem in the literature; see, e.g., [49]. It is reported in the literature and also confirmed by the authors' experience that the gradient descent converges rather fast; in most cases, 5-10 iterations are enough. For general $p \neq 1$, the gradient descent approach works as well. The case $p = 1$ amounts to considering the intrinsic median

together with the intrinsic absolute deviation. In this case, we may apply a subgradient descent which in the differentiable part amounts to rescaling the tangent vector given on the right-hand side of (27) to length 1 and considering variable step sizes which are square-integrable but not integrable; see, e.g., [5].

A speedup using the structure of the dynamic program is obtained by initializing with previous output. More precisely, when starting the iteration of the mean for data $f_{l+1:r}$, we can use the already computed mean for the data $f_{l:r}$ as an initial guess. We notice that this guess typically becomes even better the more data items we have to compute the mean for, i.e., the bigger $r - l$ is. This is important since this case is the computationally more expensive part and a good initial guess reduces the number of iterations needed.

We have the following theoretical guarantees.

Theorem 9. *In a Cartan-Hadamard manifold, the dynamic programming scheme produces a global minimizer for the univariate Mumford-Shah problem (19) and the discrete Potts problem (21), accordingly.*

A proof can be found in [117]. In this reference, also guarantees are obtained for Potts problems for general complete Riemannian manifold under additional assumptions; cf. [117, Theorem 3]. In Figure 8, the algorithm for the univariate case is illustrated for Mumford-Shah regularization for the Cartan-Hadamard manifold of positive matrices.

Multivariate Mumford-Shah and Potts problems. We now consider Mumford-Shah and Potts regularization for manifold-valued images. Even for scalar data, these problems are NP hard in dimensions higher than one even [106, 2]. Hence, finding global minimizers is not tractable anymore in the multivariate case in general. The goal is to derive approximative strategies that perform well in practice. We present a splitting approach: we rewrite (23) as the constrained problem

$$\min_{x_1, \dots, x_R} \sum_{s=1}^R \frac{1}{qR} d^q(x_s, f) + \alpha \omega_s \Psi_{a_s}(x_s) \quad \text{s. t. } x_s = x_{s+1}, s \in \{1, \dots, R\}, \quad (28)$$

with the convention $x_{R+1} = x_1$. We use a penalty method (see e.g. [18]) to obtain the unconstrained problem

$$\min_{x_1, \dots, x_R} \sum_{s=1}^R \omega_s q R \alpha \Psi_{a_s}(x_s) + d^q(x_s, f) + \mu_k d^q(x_s, x_{s+1}).$$

We use an increasing coupling sequence $(\mu_k)_k$ which fulfills the summability condition $\sum_k \mu_k^{-1/q} < \infty$. This specific splitting allows us to minimize the functional block wise, that is, with respect variables x_1, \dots, x_R separately. Performing blockwise minimization yields the algorithm

$$\begin{cases} x_1^{k+1} \in \operatorname{argmin}_x q R \omega_1 \alpha \Psi_{a_1}(x) + d^q(x, f) + \mu_k d^q(x, x_R^k), \\ x_2^{k+1} \in \operatorname{argmin}_x q R \omega_2 \alpha \Psi_{a_2}(x) + d^q(x, f) + \mu_k d^q(x, x_1^{k+1}), \\ \vdots \\ x_R^{k+1} \in \operatorname{argmin}_x q R \omega_R \alpha \Psi_{a_R}(x) + d^q(x, f) + \mu_k d^q(x, x_{R-1}^{k+1}). \end{cases} \quad (29)$$

We notice that each line of (29) decomposes into univariate subproblems of Mumford-Shah and Potts type, respectively. The subproblems are almost identical with the univariate problems above. Therefore, we can use the algorithms developed above with a few minor modification. Details may be found in [117].

There is the following result ensuring that the algorithm terminates.

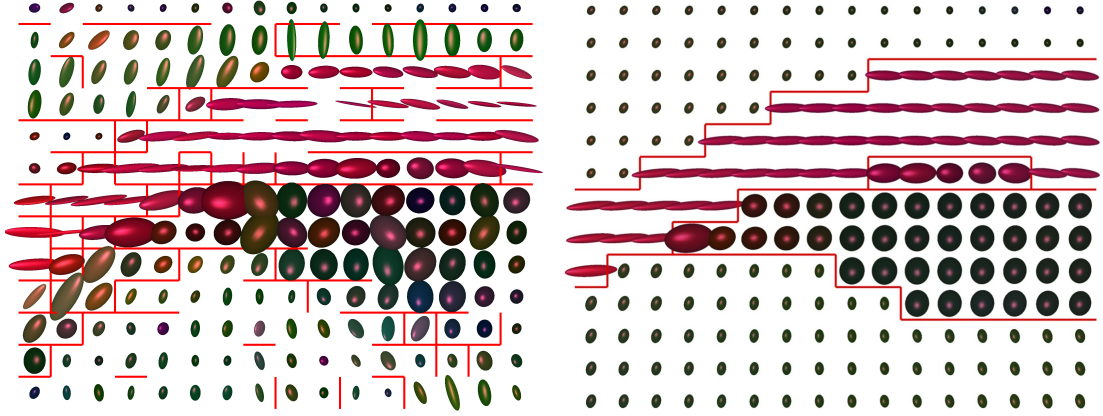


Figure 9: *Left.* Part of a corpus callosum of a human brain [39]. *Left:* Mumford-Shah regularization with $p, q = 1$. The noise is significantly reduced and the edges are preserved. Here, the edge set (depicted as red lines) of the regularization yields a segmentation.

Theorem 10. *For Cartan-Hadamard manifold-valued images the algorithm (29) for both the Mumford-Shah and the Potts problem converge.*

A proof can be found in [117].

A result of the algorithm is illustrated in Figure 9 for Mumford-Shah regularization in the Cartan-Hadamard manifold of positive matrices. The data set was taken from the Camino project [39].

5 Dealing with Indirect Measurements: Variational Regularization of Inverse Problems for Manifold Valued Data

In this section, we consider the situation when the data is not measured directly. More precisely, we consider the manifold valued analogue of the discrete inverse problem of reconstructing the signal u in the equation $\mathcal{A}u \approx f$, with given noisy data f . Here, $\mathcal{A} \in \mathbb{R}^{K \times N}$ is a matrix with unit row sums (and potentially negative items), and u is the objective to reconstruct. In the linear case, the corresponding variational model, given discrete data $f = (f_i)_{i=1}^K$, reads

$$\operatorname{argmin}_{u \in \mathbb{R}^N} \frac{1}{q} \sum_{i=1}^K \left| \sum_{j=1}^N \mathcal{A}_{i,j} u_j - f_i \right|^q + R_\alpha(u). \quad (30)$$

Here, the symbol R_α denotes a regularizing term incorporating prior assumption on the signal. The process of finding u given data f via minimizing (30) is called Tikhonov-Phillips regularization. For a general account on inverse problems and applications in imaging we refer to the books [46, 17].

In this section we consider models for variational (Tikhonov-Phillips) regularization for indirect measurement terms in the manifold setup, we present algorithms for the proposed models and we show the potential of the proposed schemes. The material is mostly taken from [94].

5.1 Models

We introduce models for variational (Tikhonov-Phillips) regularization of indirectly measured data in the manifold setup. The approach is as follows: Given a matrix $\mathcal{A} = (\mathcal{A}_{i,j})_{i,j} \in \mathbb{R}^{K \times N}$

with unit row sum, we replace the euclidean distance in $|\sum_j \mathcal{A}_{i,j} u_j - f_i|$ by the Riemannian distance $d(\cdot, f)$ in the complete, finite dimensional Riemannian manifold \mathcal{M} and the weighted mean $\sum_j \mathcal{A}_{i,j} u_j$ by the weighted Riemannian center of mass [70, 71] denoted by $\text{mean}(\mathcal{A}_{i,\cdot}, u)$ which is given by

$$\text{mean}(\mathcal{A}_{i,\cdot}, u) = \operatorname{argmin}_{v \in \mathcal{M}} \sum_j \mathcal{A}_{i,j} d(v, u_j)^2. \quad (31)$$

We consider the manifold analogue of the variational problem (30) given by

$$\operatorname{argmin}_{u \in \mathcal{M}^N} \frac{1}{q} \sum_{i=1}^K d(\text{mean}(\mathcal{A}_{i,\cdot}, u), f_i)^q + R_\alpha(u). \quad (32)$$

Here $R_\alpha(u)$ is a regularizing term, for instance

$$R_\alpha(u) = \alpha \text{TV}(u), \quad \text{or} \quad R_\alpha(u) = \text{TGV}_\alpha^2(u), \quad (33)$$

where $\text{TV}(u)$ denotes the total variation as discussed in Section 2, and $\text{TGV}_\alpha^2(u)$ denotes the total generalized variation for the discrete manifold valued target u as discussed in Section 3, for instance, the Schild variant and the parallel transport variant of TGV.

We note that also other regularizers R such as the Mumford-Shah and Potts regularizers of Section 4 and the wavelet sparse regularizers of Section 6 may be employed.

We point out that our setup includes the manifold analogue of convolution operators (a matrix with constant entries on the diagonals), e.g., modeling blur. Further, we notice that the discussion includes the multivariate setup (by serializing).

There are the following well-posedness results for the variational problems, i.e., results on the existence of minimizers. For a general regularizer R_α , under a coercivity type condition in the manifold setup the existence of a minimizer is guaranteed as the following theorem shows.

Theorem 11. *We consider a sequence of signals $(u^k)_k$ in \mathcal{M}^N and use the notation $\text{diam}(u^k)$ to denote the diameter of a single element u_k (viewed as N points in \mathcal{M}) of the sequence $\{u_k | k \in \mathbb{N}\}$. If R_α is a regularizing term such that $R_\alpha(u^k) \rightarrow \infty$, as $\text{diam}(u^k) \rightarrow \infty$, and R_α is lower semicontinuous, then the variational problem (32) with indirect measurement term has a minimizer.*

This theorem is formulated as Theorem 1 in [94] and proved there. In particular, it applies to the TV regularizers and the their analogues considering q th variation instead of total variation as well as mixed first-second order regularizers of the form $\alpha_1 \text{TV} + \alpha_0 \text{TV}^2$ with $\alpha_1 > 0$, $\alpha_0 \geq 0$.

Theorem 12. *The inverse problem (32) for manifold-valued data with TV regularizer has a minimizer. The same statement applies to mixed first and second order regularizers of the form $\alpha_1 \text{TV} + \alpha_0 \text{TV}^2$ with $\alpha_1, \alpha_0 \in [0, \infty)$, $\alpha_1 > 0$.*

This statement is part of [94, Theorem 6] and proved there. We note that, although the TGV_α^2 regularizer using either the Schild or the parallel transport variant of Section 3 is lower semicontinuous (cf. [27]) Theorem 11 does not apply. The same issue occurs with pure TV^2 regularization. To overcome this, results with weaker conditions on R and additional conditions on \mathcal{A} have been established to ensure the existence of minimizers; cf. the discussion in [94], in particular [94, Theorem 7]. The mentioned theorem applies to TGV_α^2 and pure second order TV regularizers. The conditions on \mathcal{A} are in particular fulfilled if \mathcal{A} is such that the data term fulfills the (significantly stronger) coercivity type condition

$$\sum_{i=1}^K d(\text{mean}(\mathcal{A}_{i,\cdot}, u^n), f_i)^q \rightarrow \infty, \quad \text{as} \quad \text{diam}(u^n) \rightarrow \infty. \quad (34)$$

This coercivity type condition is for instance fulfilled if \mathcal{A} fulfills the manifold analogue of lower boundedness, see [94] for details. Furthermore, the conditions hold if the underlying manifold is compact. As a result we formulate the following theorem.

Theorem 13. *Assume that either \mathcal{M} is a compact manifold, or assume that \mathcal{A} fulfills the coercivity type condition (34). Then, the inverse problem (32) for data living in \mathcal{M}^K with TGV_α^2 regularization using either the Schild or the parallel transport variant of Section 3 has a minimizer. The same statement applies to (pure) second order TV^2 regularization.*

The part of Theorem 13 concerning compact manifolds \mathcal{M} is the statement of [94, Corollary 1], the part concerning the coercivity type condition is a special case of [94, Theorem 8, Theorem 9].

5.2 Algorithmic Realization

We consider the numerical solution of (32). For differentiable data terms ($q > 1$), we build on the concept of a generalized forward backward-scheme. In the context of DTI, such a scheme has been proposed in [12]. We discuss an extension by a trajectory method and a Gauß-Seidel type update scheme which significantly improves the performance compared to the basic scheme.

Basic Generalized Forward Backward Scheme. We denote the functional in (32) by \mathcal{F} and decompose it into the data term \mathcal{D} and the regularizer R_α which we further decompose into data atoms $(\mathcal{D}_i)_i$ and regularizer atoms $(R_\alpha)_k$, i.e.,

$$\mathcal{F}(u) = \mathcal{D}(u) + R_\alpha(u) = \sum_{i=1}^K \mathcal{D}_i(u) + \sum_{l=1}^L (R_\alpha)_l(u) \quad (35)$$

with $\mathcal{D}_i(u) := \frac{1}{q} \text{d}(\text{mean}(\mathcal{A}_{i,\cdot}, u), f_i)^q$, for $i = 1, \dots, K$. Examples for decompositions $R_\alpha(u) = \sum_{l=1}^L (R_\alpha)_l(u)$ of TV and TGV_α^2 regularizers are given in Section 2 and in Section 3, respectively.

The basic idea of a generalized forward-backward scheme is to perform a gradient step for the explicit term, here \mathcal{D} , as well as a proximal mapping step for each atom of the implicit term, here $(R_\alpha)_l$. (Concerning the computation of the corresponding proximal mappings for the TV and TGV_α^2 regularizers of Sections 2 and 3, we refer to these sections.) We now focus on the data term \mathcal{D} . The gradient of \mathcal{D} w.r.t. the variable u_j , $j \in \{1, \dots, N\}$, decomposes as

$$\nabla_{u_j} \mathcal{D}(u) = \sum_{i=1}^K \nabla_{u_j} \mathcal{D}_i(u). \quad (36)$$

The gradient of \mathcal{D}_i w.r.t. u_j can then be computed rather explicitly using Jacobi fields. Performing this computation is a central topic of the paper [94]. A corresponding result is [94, Theorem 11]. The overall algorithm is summarized in Algorithm 4. Note that there, for the explicit gradient descend part, we use the k th iterate $u^k = (u_1^k, \dots, u_N^k)$ as base point for computing the gradients w.r.t. all data atoms \mathcal{D}_i , $i = 1, \dots, K$ and all items u_j , $j \in \{1, \dots, N\}$. This corresponds to a Jacobi type update scheme. During the iteration, the parameter $\lambda_k > 0$ is decreased fulfilling $\sum_k \lambda_k = \infty$ and $\sum_k \lambda_k^2 < \infty$. Recall that, for the regularizers $R_\alpha = \alpha \text{TV}$ and $R_\alpha = \text{TGV}_\alpha^2$ using either the Schild or the parallel transport variant of Section 3, the computation of line 6 in Algorithm 4 can be parallelized as explained in Section 2 and Section 3.

A Generalized Forward Backward Scheme with Gauß-Seidel Update and a Trajectory Method. A well-known issue when considering gradient descent schemes is to find a suitable parameter choice for the $(\lambda_k)_k$. Often a step size control based on line search techniques is employed. Above, there are two particular issues when employing an adaptive step size strategy: First, a single data atom $\mathcal{D}_{i'}$ may require a low step size whereas the other \mathcal{D}_i would allow for much larger steps, but in the standard form one has to use the small step size for all

Algorithm 4 FB-splitting for solving $\min_u \mathcal{D}(u) + R_\alpha(u)$

```

1: FBS( $u^0, (\lambda_k)_k$ )
2:  $k = 0$ ,
3:   repeat until stopping criterion fulfilled
4:     for  $j = 1, \dots, N$ 
5:        $u_j^{k+0.5} = \exp_{u_j^k} \left( -\lambda_k \sum_{i=1}^K \nabla_{u_j} \mathcal{D}_i(u^k) \right)$ 
6:     for  $l = 1, \dots, L$ 
7:        $u^{k+0.5+l/2L} = \text{prox}_{\lambda_k(R_\alpha)_l}(u^{k+0.5+(l-1)/2L})$ 
8:      $k \leftarrow k + 1$ 
9: return  $u^k$ 

```

Algorithm 5 FB-splitting for solving $\min_u \mathcal{D}(u) + R_\alpha(u)$ using a trajectory method

```

1: FBSTraj( $u^0, (\lambda_k)_k$ )
2:  $k = 0$ ,
3:   repeat until stopping criterion fulfilled
4:     for  $i = 1, \dots, K$ 
5:        $u^{k+i/2K} = \text{traj}_{\lambda_k \mathcal{D}_i}(u^{k+(i-1)/2K})$ 
6:     for  $l = 1, \dots, L$ 
7:        $u^{k+0.5+l/2L} = \text{prox}_{\lambda_k(R_\alpha)_l}(u^{k+0.5+(l-1)/2L})$ 
8:      $k \leftarrow k + 1$ 
9: return  $x^k$ 

```

\mathcal{D}_i . Second, a small stepsize restriction from a single $\mathcal{D}_{i'}$ also yields a small stepsize in the the proximal mapping for the regularization terms. Together, a small step size within an atom of the data term results in a small step size for the whole loop of the iteration Algorithm 4.

In order to overcome these step size issue, the paper [94] proposes to employ a Gauss-Seidel type update scheme together with a trajectory method. To explain the idea, we first replace the update of lines 4/5 of Algorithm 4 by

$$\begin{cases} \text{for } i = 1, \dots, K \\ \text{for } j = 1, \dots, N \\ u_j^{k+i/2K} = \exp_{u_j^{k+(i-1)/2K}} \left(-\lambda_k \nabla_{u_j} \mathcal{D}_i(u^{k+(i-1)/2K}) \right). \end{cases} \quad (37)$$

Here, the computation of the gradients is performed in a cyclic way w.r.t. the \mathcal{D}_i which corresponds to a Gauß-Seidel type update scheme. This in particular has the following advantage: if we face a small step size for a particular $\mathcal{D}_{i'}$, instead of decreasing the step size for the whole loop, we may employ the following *trajectory method*. Instead of using a single geodesic line for the decay w.r.t. the atom \mathcal{D}_i at iteration k , we follow a polygonal geodesic path. That is, at iteration k , we do not only carry out a single but possibly multiple successive gradient descent steps w.r.t. \mathcal{D}_i , where the length of each step is chosen optimal for the current direction for \mathcal{D}_i (by a line search strategy) and the descent steps are iterated until the sum of the step “times” for \mathcal{D}_i reaches λ_k . Details can be found in [94]. This way, a global step size choice with all atoms (potentially negatively) influencing each other, is replaced by an autonomous step size choice for each atom. We denote the resulting operator by $\text{traj}_{\lambda_k \mathcal{D}_i}$ for a data atom \mathcal{D}_i . The overall algorithm is subsumed in Algorithm 5.

We point out that also a stochastic variant of this scheme where the atoms are chosen in a random order has been proposed in [94]. Finally, we point out that it is also possible to employ

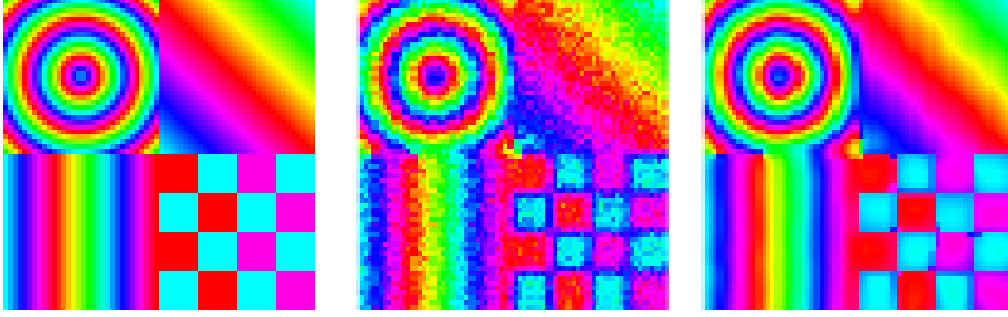


Figure 10: Deconvolving an \mathbb{S}^1 -valued image (visualized as hue values.) As input data (*center*) we use the ground truth (*left*) convolved with a Gaussian kernel (5×5 kernel with $\sigma = 1$) and corrupted by von Mises noise. We observe the denoising and deblurring capabilities of TGV regularized deconvolution (*right*.)

a CPPA or a PPPA as explained in Section 2. This is in particular important if the data term is not differentiable, i.e., if $q = 1$. For details on computing the proximal mappings of the atoms \mathcal{D}_i we refer to the paper [94].

We illustrate the results of joint deconvolution and denoising of manifold-valued data in Figure 10. The data consists of an \mathbb{S}^1 -valued image convolved with a Gaussian kernel and corrupted by von Mises noise. We employ S-TGV_α^2 regularized deconvolution and observe good denoising and deblurring capabilities.

6 Wavelet Sparse Regularization of Manifold Valued Data

In contrast to TV, higher order TV type and Mumford-Shah regularizers which are all based on differences (or derivatives in the continuous setting), we here consider a variational scheme employing manifold valued interpolatory wavelets in the regularizing term. In particular, we consider a sparsity promoting ℓ^1 type term as well as an ℓ^0 type term. We obtain results on the existence of minimizers for the proposed models. We provide algorithms for the proposed models and show the potential of the proposed algorithms.

Interpolatory wavelet transforms for linear space data have been investigated by D. Donoho in [42]. Their analogues for manifold-valued data have been introduced by Ur Rahman, Donoho and their coworkers in [105]. Such transforms have been analyzed and developed further in [64, 62, 115]. Typically, the wavelet-type transforms employ an (interpolatory) subdivision scheme to predict the signal on a finer scale. The ‘difference’ between the prediction and the actual data on the finer scale is realized by vectors living in the tangent spaces of the predicted signal points which point to the actual signal values, i.e., they yield actual signal values after application of a retraction such as the exponential map. These tangent vectors then serve as detail coefficients. Subdivision schemes for manifold-valued data have been considered in [109, 61, 121, 114, 110]. Interpolatory wavelet transforms and subdivision are discussed in more detail in [108]. All the above approaches consider explicit schemes, i.e., the measured data is processed in a forward way using the analogues of averaging rules and differences in the manifold setting. In contrast, we here consider an implicit approach based on a variational formulation.

6.1 Model

We discuss a model for wavelet sparse regularization for manifold-valued data. For the reader's convenience, we consider the univariate situation here. For the multivariate setup and further details we refer to [95]. Let $f \in \mathcal{M}^K$ be data in the complete, finite dimensional Riemannian manifold \mathcal{M} . We consider the problem

$$\operatorname{argmin}_{u \in \mathcal{M}^N} \frac{1}{q} d(\mathcal{A}(u), f)^q + \mathcal{W}_\alpha^{\mu, p}(u). \quad (38)$$

Here, u denotes the argument to optimize for; it may be thought of as the underlying signal generating the response $\mathcal{A}(u) \in \mathcal{M}^K$, where \mathcal{A} is an operator which models a system's response, for instance. In case of pure denoising, \mathcal{A} is the identity on \mathcal{M}^N , $N = K$. Further instances of \mathcal{A} are the manifold valued analogues of convolution operators as pointed out in Section 5. The deviation of $\mathcal{A}(u)$ from f is quantified by $\frac{1}{q} d(\mathcal{A}(u), f)^q = \frac{1}{q} \sum_{i=1}^K d(\mathcal{A}(u)_i, f_i)^q$. Further, $\alpha = (\alpha_1, \alpha_2)$ is a parameter vector regulating the trade-off between the data fidelity, and the regularizing term $\mathcal{W}_\alpha^{\mu, p}$ which is the central topic of this section and is given by

$$\mathcal{W}_\alpha^{\mu, p}(u) = \alpha_1 \cdot \sum_{n, r} 2^{rp(\mu + \frac{1}{2} - \frac{1}{p})} \|d_{n, r}(u)\|_{\hat{u}_{n, r}}^p + \alpha_2 \cdot \sum_n d(\tilde{u}_{n-1, 0}, \tilde{u}_{n, 0})^p. \quad (39)$$

We discuss the regularizing term (39) in more detail in the following. We start with the so-called detail coefficients $d_{n, r}$ which requires some space. The details $d_{n, r}$ at scale r of the interpolatory wavelet transform for manifold valued data are given by

$$d_{n, r} = d_{n, r}(u) = 2^{-r/2} (\tilde{u}_{n, r} \ominus \hat{u}_{n, r}), \quad \hat{u}_{n, r} = S\tilde{u}_{n, r-1}. \quad (40)$$

Here $\tilde{u}_{n, r-1} = u_{2^{R-r+1}n}$ and $\tilde{u}_{n, r} = u_{2^{R-r}n}$ (with R the finest level) denote the thinned out target u at scale $r-1$ and r , respectively. The coarsest level is denoted by $\tilde{u}_{n, 0} = u_{2^R n}$. The symbol \ominus takes the Riemannian logarithm of the first argument w.r.t. the second argument as base point. $S\tilde{u}_{n, r-1}$ denotes the application of an interpolatory subdivision scheme S for manifold-valued data to the coarse level data $\tilde{u}_{\cdot, r-1}$ evaluated at the index n which serves as prediction for $\tilde{u}_{n, r}$, i.e.,

$$S\tilde{u}_{n, r-1} = \operatorname{mean}(s_{n-2}, \dots, \tilde{u}_{\cdot, r-1}). \quad (41)$$

Here the mask s of the subdivision scheme S is a real-valued sequence such that the even as well as the odd entries sum up to 1. The even and the odd entries yield two sets of weights; in case of an interpolatory scheme $s_0 = 1$ and all other even weights equal zero. The simplest example of an interpolatory scheme is the linear interpolatory scheme for which $s_{-1} = s_1 = 1/2$ and the other odd weights equal zero. Thus, in the manifold setup, the prediction of the linear interpolatory consists of the geodesic midpoint between two consecutive coarse level items. The linear interpolatory scheme is a particular example of the interpolatory Deslaurier-Dubuc schemes whose third order variant is given by the coefficients $s_{-3} = s_3 = -1/16$ as well as $s_{-1} = s_1 = 9/16$ with the remaining odd coefficients equal to zero. A reference on linear subdivision schemes is the book [29]; for manifold-valued schemes we refer to references above.

Coming back to (40), the detail $d_{n, r}$ quantifies the deviation between the prediction $S\tilde{u}_{n, r-1}$ and the actual r th level data item $\tilde{u}_{n, r}$ by

$$d_{n, r} = \tilde{u}_{n, r} \ominus S\tilde{u}_{n, r-1} = \exp_{S\tilde{u}_{n, r-1}}^{-1} \tilde{u}_{n, r}$$

which denotes the tangent vector sitting in $\hat{u}_{n, r} = S\tilde{u}_{n, r-1}$ pointing to $\tilde{u}_{n, r}$.

With this information on the details $d_{n,r}$, we come back to the definition of the regularizer in (39). We observe that the symbol $\|\cdot\|_{\hat{u}_{n,r}}$ denotes the norm induced by the Riemannian scalar product in the point $\hat{u}_{n,r}$, which is the point where the detail $d_{n,r}(u)$ is a tangent vector at; it measures the size of the detail. The parameter μ is a smoothness parameter and the parameter $p \geq 1$ stems from a norm type term. The second term addresses measures the p th power of the distance between neighboring items on the coarsest scale.

We emphasize that the case $p = 1, \mu = 1$ in (38), corresponds to the manifold analogue of the LASSO [103, 33] or ℓ^1 -sparse regularization which, in the linear case, is addressed by (iterative) soft thresholding [43]. This case is particularly interesting since it promotes solutions u which are likely to be sparse w.r.t. the considered wavelet expansion.

The manifold analogue of ℓ^0 -sparse regularization which actually measures sparsity is obtained by using the regularizer

$$\mathcal{W}_\alpha^0(u) = \alpha_1 \# \{(n, r) : d_{n,r}(u) \neq 0\} + \alpha_2 \# \{n : \tilde{u}_{n-1,0} \neq \tilde{u}_{n,0}\}. \quad (42)$$

The operator $\#$ is used to count the number of elements in the corresponding set. Note that this way the number of non-zero detail coefficients of the wavelet expansion is penalized. Similar to the linear case [113, 43, 33], potential applications of the considered sparse regularization techniques are denoising and compression.

Concerning the existence of minimizers, we have the following results.

Theorem 14. *The variational problem (38) of wavelet regularization using the regularizers $\mathcal{W}_\alpha^{\mu,p}$ of (39) with $\alpha_2 \neq 0$ has a minimizer.*

Similar to the existence results in Section 5 these results are based on showing lower semi-continuity and a coercivity type condition in the manifold setting. To ensure a coercivity type condition when $\alpha_2 = 0$ we need to impose additional conditions on \mathcal{A} . For a precise discussion of this point we refer to [95]. As in Section 5 we here state a special case which is easier to access.

Theorem 15. *Let \mathcal{M} be a compact manifold, or assume that \mathcal{A} fulfills the coercivity type condition (34). The variational problem (38) of wavelet regularization using the regularizers $\mathcal{W}_\alpha^{\mu,p}$ of (39) with $\alpha_2 = 0$ has a minimizer.*

Theorem 16. *We make the same assumptions as in Theorem 15. Then wavelet sparse regularization using the ℓ^0 type regularizing terms $\mathcal{W}_\alpha^0(u)$ of (42) has a minimizer.*

For proofs of these theorems (whereby Theorem 15 is a special case of [95, Theorem 4]) we refer to [95].

6.2 Algorithmic Realization

We decompose the regularizer $\mathcal{W}_\alpha^{\mu,p}$ into atoms \mathcal{R}_k with a enumerating index k by

$$\mathcal{R}_k = \alpha_1 \sum_{n,r} 2^{rp\left(\mu + \frac{1}{2} - \frac{1}{p}\right)} \|d_{n,r}(u)\|_{\hat{u}_{n,r}}^p, \quad \text{or} \quad \mathcal{R}_k = \alpha_2 d(\tilde{u}_{n-1,0}, \tilde{u}_{n,0})^p, \quad (43)$$

and the data term into atoms \mathcal{D}_k according to (35). To these atoms we may apply the concepts of a generalized forward backward-scheme with Gauss-Seidel type update and a trajectory method (explained in Section 5) as well as the concept of a CPPA or a PPPA (explained in Section 2). To implement these schemes expressions for the (sub)gradients and proximal mappings of the atoms \mathcal{R}_k based on Jacobi fields have been derived in [95]. Due to space reasons, we do not elaborate on this derivation here, but refer to the mentioned paper for details. Similar to (43), we may

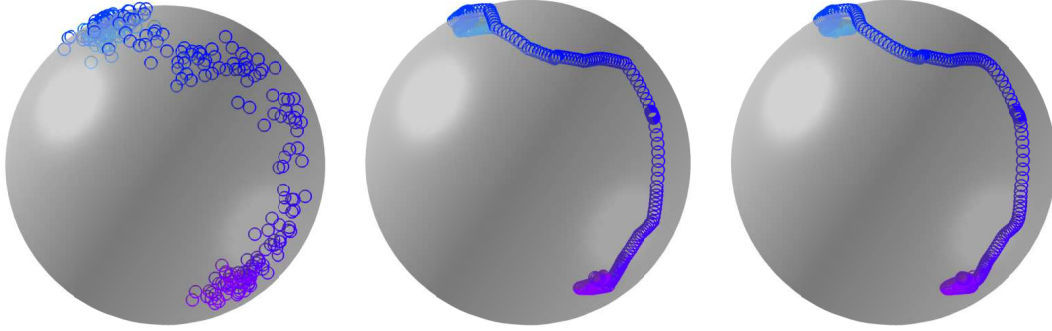


Figure 11: Illustration of the proposed ℓ^1 wavelet regularization for a \mathbb{S}^2 -valued time series. The given data (*left*) is noisy and blurred with the manifold analogue of a Gaussian kernel with $\sigma = 2$. We display the result of using the first order interpolatory wavelet (*middle*) and the third order Deslaurier-Dubuc (DD) wavelet (*right*).

decompose the ℓ^0 -sparse regularizer \mathcal{W}_α^0 into atoms we also denote by \mathcal{D}_k , and apply a CPPA or PPPA. For details we refer to [95]. We illustrate ℓ^1 wavelet regularization by considering a joint deblurring and denoising problem for an \mathbb{S}^2 -valued time series in Figure 11. The noisy data is convolved with the manifold-valued analogue of a discrete Gaussian kernel. As prediction operator we employ the linear interpolatory subdivision scheme which inserts the geodesic midpoint as well as the cubic Deslaurier Dubuc scheme for manifold valued data as explained above.

Acknowledgements

MH acknowledges support by the Austrian Science Fund (FWF) (Grant J 4112). AW acknowledges support by the DFG Grants WE 5886/3-1 and WE 5886/4-1.

References

- [1] B. Afsari, R. Tron, and R. Vidal. On the convergence of gradient descent for finding the Riemannian center of mass. *SIAM Journal on Control and Optimization*, 51(3):2230–2260, 2013.
- [2] B. Alexeev and R. Ward. On the complexity of Mumford–Shah-type regularization, viewed as a relaxed sparsity constraint. *IEEE Transactions on Image Processing*, 19(10):2787–2789, 2010.
- [3] S. Alliney. Digital filters as absolute norm regularizers. *IEEE Transactions on Signal Processing*, 40:1548–1562, 1992.
- [4] L. Ambrosio and V. M. Tortorelli. Approximation of functional depending on jumps by elliptic functional via Γ -convergence. *Communications on Pure and Applied Mathematics*, 43(8):999–1036, 1990.
- [5] M. Arnaudon and F. Nielsen. On approximating the Riemannian 1-center. *Computational Geometry*, 46(1):93–104, 2013.

- [6] D. Azagra and J. Ferrera. Proximal calculus on Riemannian manifolds. *Mediterranean Journal of Mathematics*, 2:437–450, 2005.
- [7] M. Bačák. Computing medians and means in Hadamard spaces. *SIAM Journal on Optimization*, 24(3):1542–1566, 2014.
- [8] M. Bačák. *Convex analysis and optimization in Hadamard spaces*. de Gruyter, 2014.
- [9] M. Bačák, R. Bergmann, G. Steidl, and A. Weinmann. A second order non-smooth variational model for restoring manifold-valued images. *SIAM Journal on Scientific Computing*, 38(1):A567–A597, 2016.
- [10] P. Basser, J. Mattiello, and D. LeBihan. MR diffusion tensor spectroscopy and imaging. *Biophysical Journal*, 66(1):259–267, 1994.
- [11] M. Baust, L. Demaret, M. Storath, N. Navab, and A. Weinmann. Total variation regularization of shape signals. In *IEEE Conference on Computer Vision and Pattern Recognition (CVPR)*, pages 2075–2083, 2015.
- [12] M. Baust, A. Weinmann, M. Wieczorek, T. Lasser, M. Storath, and N. Navab. Combined tensor fitting and TV regularization in diffusion tensor imaging based on a Riemannian manifold approach. *IEEE Transactions on Medical Imaging*, 35(8):1972–1989, 2016.
- [13] R. Bergmann, R. H. Chan, R. Hielscher, J. Persch, and G. Steidl. Restoration of manifold-valued images by half-quadratic minimization. *Inverse Problems and Imaging*, 10:281304, 2016.
- [14] R. Bergmann, J. H. Fitschen, J. Persch, and G. Steidl. Infimal convolution type coupling of first and second order differences on manifold-valued images. *Scale Space and Variational Methods in Computer Vision 2017*, pages 447–459, 2017.
- [15] R. Bergmann, J. H. Fitschen, J. Persch, and G. Steidl. Priors with coupled first and second order differences for manifold-valued image processing. *Journal of mathematical imaging and vision*, 60(9):1459–1481, 2018.
- [16] B. Berkels, P. Fletcher, B. Heeren, M. Rumpf, and B. Wirth. Discrete geodesic regression in shape space. In *International Workshop on Energy Minimization Methods in Computer Vision and Pattern Recognition*, pages 108–122. Springer, 2013.
- [17] M. Bertero and P. Boccacci. *Introduction to inverse problems in imaging*. CRC press, 1998.
- [18] D. Bertsekas. Multiplier methods: a survey. *Automatica*, 12(2):133–145, 1976.
- [19] D. Bertsekas. Incremental proximal methods for large scale convex optimization. *Mathematical Programming*, 129:163–195, 2011.
- [20] A. Blake and A. Zisserman. *Visual reconstruction*. MIT press Cambridge, 1987.
- [21] C. Boyer, A. Chambolle, Y. D. Castro, V. Duval, F. De Gournay, and P. Weiss. On representer theorems and convex regularization. *SIAM Journal on Optimization*, 29(2):1260–1281, 2019.
- [22] Y. Boykov, O. Veksler, and R. Zabih. Fast approximate energy minimization via graph cuts. *IEEE Transactions on Pattern Analysis and Machine Intelligence*, 23(11):1222–1239, 2001.

- [23] L. Boysen, A. Kempe, V. Liebscher, A. Munk, and O. Wittich. Consistencies and rates of convergence of jump-penalized least squares estimators. *The Annals of Statistics*, 37(1):157–183, 2009.
- [24] K. Bredies and M. Carioni. Sparsity of solutions for variational inverse problems with finite-dimensional data. *arXiv preprint arXiv:1809.05045*, 2018.
- [25] K. Bredies and M. Holler. Regularization of linear inverse problems with total generalized variation. *Journal of Inverse and Ill-Posed Problems*, 22(6):871–913, 2014.
- [26] K. Bredies, M. Holler, M. Storath, and A. Weinmann. An observation concerning the parallel transport variant of total generalized variation for manifold-valued data. *Oberwolfach Report*, 20:38–41, 2018.
- [27] K. Bredies, M. Holler, M. Storath, and A. Weinmann. Total Generalized Variation for manifold-valued data. *SIAM Journal on Imaging Sciences*, 11(3):1785–1848, 2018.
- [28] K. Bredies, K. Kunisch, and T. Pock. Total generalized variation. *SIAM Journal on Imaging Sciences*, 3(3):492–526, 2010.
- [29] A. S. Cavaretta, W. Dahmen, and C. A. Micchelli. *Stationary subdivision*, volume 453. American Mathematical Soc., 1991.
- [30] A. Chambolle. Image segmentation by variational methods: Mumford and Shah functional and the discrete approximations. *SIAM Journal on Applied Mathematics*, 55(3):827–863, 1995.
- [31] A. Chambolle. Finite-differences discretizations of the Mumford-Shah functional. *ESAIM: Mathematical Modelling and Numerical Analysis*, 33(02):261–288, 1999.
- [32] A. Chambolle. An algorithm for total variation minimization and applications. *Journal of Mathematical Imaging and Vision*, 20:89–97, 2004.
- [33] A. Chambolle, R. De Vore, N. Lee, and B. Lucier. Nonlinear wavelet image processing: variational problems, compression, and noise removal through wavelet shrinkage. *IEEE Transactions on Image Processing*, 7(3):319–335, 1998.
- [34] A. Chambolle and P.-L. Lions. Image recovery via total variation minimization and related problems. *Numerische Mathematik*, 76(2):167–188, 1997.
- [35] A. Chambolle and T. Pock. A first-order primal-dual algorithm for convex problems with applications to imaging. *Journal of Mathematical Imaging and Vision*, 40:120–145, 2011.
- [36] T. Chan and S. Esedoglu. Aspects of total variation regularized L^1 function approximation. *SIAM Journal on Applied Mathematics*, 65:1817–1837, 2005.
- [37] T. Chan, S. Kang, and J. Shen. Total variation denoising and enhancement of color images based on the CB and HSV color models. *Journal of Visual Communication and Image Representation*, 12:422–435, 2001.
- [38] G. Cheng, H. Salehian, and B. Vemuri. Efficient recursive algorithms for computing the mean diffusion tensor and applications to DTI segmentation. In *Computer Vision–ECCV 2012*, pages 390–401. Springer, 2012.

- [39] P. Cook, Y. Bai, S. Nadjati-Gilani, K. Seunarine, M. Hall, G. Parker, and D. Alexander. Camino: Open-source diffusion-MRI reconstruction and processing. In *14th Scientific Meeting of the International Society for Magnetic Resonance in Medicine*, page 2759, 2006.
- [40] D. Cremers and E. Strekalovskiy. Total cyclic variation and generalizations. *Journal of Mathematical Imaging and Vision*, 47(3):258–277, 2013.
- [41] F. Demengel. Fonctions a hessien borné. In *Annales de l’institut Fourier*, volume 34, pages 155–190, 1984.
- [42] D. Donoho. Interpolating wavelet transforms. *Preprint, Department of Statistics, Stanford University*, 2(3), 1992.
- [43] D. Donoho. De-noising by soft-thresholding. *IEEE Transactions on Information Theory*, 41(3):613–627, 1995.
- [44] T. Drummond and R. Cipolla. Real-time visual tracking of complex structures. *IEEE Transactions on Pattern Analysis and Machine Intelligence*, 24:932–946, 2002.
- [45] J. Duran, M. Möller, C. Sbert, and D. Cremers. Collaborative total variation: a general framework for vectorial tv models. *SIAM Journal on Imaging Sciences*, 9(1):116–151, 2016.
- [46] H. W. Engl, M. Hanke, and A. Neubauer. *Regularization of inverse problems*, volume 375. Springer Science & Business Media, 1996.
- [47] O. Ferreira and P. Oliveira. Subgradient algorithm on riemannian manifolds. *Journal of Optimization Theory and Applications*, 97(1):93–104, 1998.
- [48] O. Ferreira and P. Oliveira. Proximal point algorithm on Riemannian manifolds. *Optimization*, 51:257–270, 2002.
- [49] R. Ferreira, J. Xavier, J. Costeira, and V. Barroso. Newton algorithms for Riemannian distance related problems on connected locally symmetric manifolds. *IEEE Journal of Selected Topics in Signal Processing*, 7:634–645, 2013.
- [50] P. Fletcher and S. Joshi. Riemannian geometry for the statistical analysis of diffusion tensor data. *Signal Processing*, 87:250–262, 2007.
- [51] M. Fornasier, R. March, and F. Solombrino. Existence of minimizers of the Mumford-Shah functional with singular operators and unbounded data. *Annali di Matematica Pura ed Applicata*, 192(3):361–391, 2013.
- [52] M. Fornasier and R. Ward. Iterative thresholding meets free-discontinuity problems. *Foundations of Computational Mathematics*, 10(5):527–567, 2010.
- [53] F. Friedrich, A. Kempe, V. Liebscher, and G. Winkler. Complexity penalized M-estimation. *Journal of Computational and Graphical Statistics*, 17(1):201–224, 2008.
- [54] S. Geman and D. Geman. Stochastic relaxation, Gibbs distributions, and the Bayesian restoration of images. *IEEE Transactions on Pattern Analysis and Machine Intelligence*, 6(6):721–741, 1984.
- [55] P. Getreuer. Rudin-Osher-Fatemi total variation denoising using split Bregman. *Image Processing On Line*, 2012. <http://dx.doi.org/10.5201/ipol.2012.g-tvd>.

- [56] M. Giaquinta, G. Modica, and J. Souček. Variational problems for maps of bounded variation with values in S^1 . *Calculus of Variations and Partial Differential Equations*, 1(1):87–121, 1993.
- [57] M. Giaquinta and D. Mucci. The BV-energy of maps into a manifold: relaxation and density results. *Annali della Scuola Normale Superiore di Pisa-Classe di Scienze*, 5(4):483–548, 2006.
- [58] T. Goldstein and S. Osher. The split Bregman method for L^1 -regularized problems. *SIAM Journal on Imaging Sciences*, 2:323–343, 2009.
- [59] Y. Gousseau and J.-M. Morel. Are natural images of bounded variation? *SIAM Journal on Mathematical Analysis*, 33:634–648, 2001.
- [60] P. Green and K. Mardia. Bayesian alignment using hierarchical models, with applications in protein bioinformatics. *Biometrika*, 93:235–254, 2006.
- [61] P. Grohs. Smoothness analysis of subdivision schemes on regular grids by proximity. *SIAM Journal on Numerical Analysis*, 46(4):2169–2182, 2008.
- [62] P. Grohs. Stability of manifold-valued subdivision schemes and multiscale transformations. *Constructive Approximation*, 32(3):569–596, 2010.
- [63] P. Grohs and M. Sprecher. Total variation regularization on Riemannian manifolds by iteratively reweighted minimization. *Information and Inference*, 5(4):353–378, 2016.
- [64] P. Grohs and J. Wallner. Interpolatory wavelets for manifold-valued data. *Applied and Computational Harmonic Analysis*, 27(3):325–333, 2009.
- [65] W. Hinterberger and O. Scherzer. Variational methods on the space of functions of bounded Hessian for convexification and denoising. *Computing*, 76(1-2):109–133, 2006.
- [66] K. Hohm, M. Storath, and A. Weinmann. An algorithmic framework for Mumford-Shah regularization of inverse problems in imaging. *Inverse Problems*, 2015. to appear.
- [67] J. Itoh and M. Tanaka. The dimension of a cut locus on a smooth Riemannian manifold. *Tohoku Mathematical Journal, Second Series*, 50(4):571–575, 1998.
- [68] M. Jiang, P. Maass, and T. Page. Regularizing properties of the Mumford-Shah functional for imaging applications. *Inverse Problems*, 30(3):035007, 2014.
- [69] H. Johansen-Berg and T. Behrens. *Diffusion MRI: From quantitative measurement to in-vivo neuroanatomy*. Academic Press, London, 2009.
- [70] H. Karcher. Riemannian center of mass and mollifier smoothing. *Communications on Pure and Applied Mathematics*, 30:509–541, 1977.
- [71] W. Kendall. Probability, convexity, and harmonic maps with small image I: uniqueness and fine existence. *Proceedings of the London Mathematical Society*, 3:371–406, 1990.
- [72] A. Kheyfets, W. A. Miller, and G. A. Newton. Schild’s ladder parallel transport procedure for an arbitrary connection. *Internat. J. Theoret. Phys.*, 39(12):2891–2898, 2000.
- [73] R. Killick, P. Fearnhead, and I. Eckley. Optimal detection of changepoints with a linear computational cost. *Journal of the American Statistical Association*, 107(500):1590–1598, 2012.

- [74] J. Lellmann, E. Strekalovskiy, S. Koetter, and D. Cremers. Total variation regularization for functions with values in a manifold. In *International Conference on Computer Vision (ICCV)*, pages 2944–2951, 2013.
- [75] M. Lorenzi and X. Pennec. Efficient parallel transport of deformations in time series of images: from schilds to pole ladder. *Journal of mathematical imaging and vision*, 50(1-2):5–17, 2014.
- [76] D. Massonnet and K. Feigl. Radar interferometry and its application to changes in the earth’s surface. *Reviews of Geophysics*, 36(4):441–500, 1998.
- [77] P. Michor and D. Mumford. An overview of the Riemannian metrics on spaces of curves using the Hamiltonian approach. *Applied and Computational Harmonic Analysis*, 23(1):74 – 113, 2007.
- [78] J.-J. Moreau. Fonctions convexes duales et points proximaux dans un espace hilbertien. *Comptes Rendus de l’Académie des Sciences. Series A Mathematics.*, 255:2897–2899, 1962.
- [79] D. Mumford and J. Shah. Boundary detection by minimizing functionals. In *IEEE Conference on Computer Vision and Pattern Recognition*, volume 17, pages 137–154, 1985.
- [80] D. Mumford and J. Shah. Optimal approximations by piecewise smooth functions and associated variational problems. *Communications on Pure and Applied Mathematics*, 42(5):577–685, 1989.
- [81] M. Nikolova. Minimizers of cost-functions involving nonsmooth data-fidelity terms. Application to the processing of outliers. *SIAM Journal on Numerical Analysis*, 40:965–994, 2002.
- [82] M. Nikolova. A variational approach to remove outliers and impulse noise. *Journal of Mathematical Imaging and Vision*, 20:99–120, 2004.
- [83] X. Pennec, P. Fillard, and N. Ayache. A Riemannian framework for tensor computing. *International Journal of Computer Vision*, 66:41–66, 2006.
- [84] T. Pock, D. Cremers, H. Bischof, and A. Chambolle. An algorithm for minimizing the Mumford-Shah functional. In *IEEE International Conference on Computer Vision and Pattern Recognition*, pages 1133–1140, 2009.
- [85] R. Potts. Some generalized order-disorder transformations. *Mathematical Proceedings of the Cambridge Philosophical Society*, 48(01):106–109, 1952.
- [86] R. Rezakhanlou, A. Agianniotis, J. Schrauwen, A. Griffo, D. Sage, C. Bouten, F. Van de Vosse, M. Unser, and N. Stergiopoulos. Experimental investigation of collagen waviness and orientation in the arterial adventitia using confocal laser scanning microscopy. *Biomechanics and Modeling in Mechanobiology*, 11:461–473, 2012.
- [87] F. Rocca, C. Prati, and A. Ferretti. An overview of SAR interferometry. In *Proceedings of the 3rd ERS Symposium on Space at the Service of our Environment, Florence*, 1997.
- [88] P. Rodriguez and B. Wohlberg. An iteratively reweighted norm algorithm for total variation regularization. In *IEEE Conference on Signals, Systems and Computers*, pages 892–896, 2006.

- [89] G. Rosman, M. Bronstein, A. Bronstein, A. Wolf, and R. Kimmel. Group-valued regularization framework for motion segmentation of dynamic non-rigid shapes. In *Scale Space and Variational Methods in Computer Vision*, pages 725–736. Springer, 2012.
- [90] L. Rudin, S. Osher, and E. Fatemi. Nonlinear total variation based noise removal algorithms. *Physica D: Nonlinear Phenomena*, 60(1):259–268, 1992.
- [91] G. Sapiro and D. L. Ringach. Anisotropic diffusion of multivalued images with applications to color filtering. *IEEE transactions on image processing*, 5(11):1582–1586, 1996.
- [92] A. Stefanoiu, A. Weinmann, M. Storath, N. Navab, and M. Baust. Joint segmentation and shape regularization with a generalized forward–backward algorithm. *IEEE Transactions on Image Processing*, 25(7):3384–3394, 2016.
- [93] M. Storath and A. Weinmann. Fast partitioning of vector-valued images. *SIAM Journal on Imaging Sciences*, 7(3):1826–1852, 2014.
- [94] M. Storath and A. Weinmann. Variational regularization of inverse problems for manifold-valued data. *arXiv preprint arXiv:1804.10432*, 2018.
- [95] M. Storath and A. Weinmann. Wavelet sparse regularization for manifold-valued data. *arXiv preprint arXiv:1808.00505*, 2018.
- [96] M. Storath, A. Weinmann, and L. Demaret. Jump-sparse and sparse recovery using Potts functionals. *IEEE Transactions on Signal Processing*, 62(14):3654–3666, 2014.
- [97] M. Storath, A. Weinmann, J. Friel, and M. Unser. Joint image reconstruction and segmentation using the Potts model. *Inverse Problems*, 31(2):025003, 2014.
- [98] M. Storath, A. Weinmann, and M. Unser. Exact algorithms for L^1 -TV regularization of real-valued or circle-valued signals. *SIAM Journal on Scientific Computing*, 38(1):A614–A630, 2016.
- [99] M. Storath, A. Weinmann, and M. Unser. Jump-penalized least absolute values estimation of scalar or circle-valued signals. *Information and Inference*, 6(3):225–245, 2017.
- [100] E. Strelakoskiy and D. Cremers. Total variation for cyclic structures: Convex relaxation and efficient minimization. In *IEEE Conference on Computer Vision and Pattern Recognition (CVPR)*, pages 1905–1911, 2011.
- [101] D. Strong and T. Chan. Edge-preserving and scale-dependent properties of total variation regularization. *Inverse Problems*, 19:S165, 2003.
- [102] K. Thiel, X. Wu, and P. Hartl. ERS-tandem-interferometric observation of volcanic activities in Iceland. *ESA SP*, pages 475–480, 1997.
- [103] R. Tibshirani. Regression shrinkage and selection via the lasso. *Journal of the Royal Statistical Society. Series B (Methodological)*, pages 267–288, 1996.
- [104] A. Tsai, A. Yezzi Jr, and A. Willsky. Curve evolution implementation of the Mumford-Shah functional for image segmentation, denoising, interpolation, and magnification. *IEEE Transactions on Image Processing*, 10(8):1169–1186, 2001.
- [105] I. Ur Rahman, V. Drori, I. Stodden, D. Donoho, and P. Schröder. Multiscale representations for manifold-valued data. *Multiscale Modeling & Simulation*, 4(4):1201–1232, 2005.

- [106] O. Veksler. *Efficient graph-based energy minimization methods in computer vision*. PhD thesis, Cornell University, 1999.
- [107] T. Vogt, E. Strekalovskiy, D. Cremers, and J. Lellmann. Lifting methods for manifold-valued variational problems. *arXiv preprint arXiv:1908.03776*, 2019.
- [108] J. Wallner. Geometric subdivision and multiscale transforms. *arXiv preprint arXiv:1907.07550*, 2019.
- [109] J. Wallner and N. Dyn. Convergence and C^1 analysis of subdivision schemes on manifolds by proximity. *Computer Aided Geometric Design*, 22(7):593–622, 2005.
- [110] J. Wallner, E. Yazdani, and A. Weinmann. Convergence and smoothness analysis of subdivision rules in Riemannian and symmetric spaces. *Advances in Computational Mathematics*, 34(2):201–218, 2011.
- [111] Z. Wang and B. Vemuri. An affine invariant tensor dissimilarity measure and its applications to tensor-valued image segmentation. In *IEEE Conference on Computer Vision and Pattern Recognition.*, pages I228–I233, 2004.
- [112] Z. Wang and B. Vemuri. DTI segmentation using an information theoretic tensor dissimilarity measure. *IEEE Transactions on Medical Imaging*, 24(10):1267–1277, 2005.
- [113] J. Weaver, Y. Xu, D. Healy, and L. Cromwell. Filtering noise from images with wavelet transforms. *Magnetic Resonance in Medicine*, 21(2):288–295, 1991.
- [114] A. Weinmann. Nonlinear subdivision schemes on irregular meshes. *Constructive Approximation*, 31(3):395–415, 2010.
- [115] A. Weinmann. Interpolatory multiscale representation for functions between manifolds. *SIAM Journal on Mathematical Analysis*, 44:162–191, 2012.
- [116] A. Weinmann, L. Demaret, and M. Storath. Total variation regularization for manifold-valued data. *SIAM Journal on Imaging Sciences*, 7(4):2226–2257, 2014.
- [117] A. Weinmann, L. Demaret, and M. Storath. Mumford–Shah and Potts regularization for manifold-valued data. *Journal of Mathematical Imaging and Vision*, 55(3):428–445, 2016.
- [118] A. Weinmann, M. Storath, and L. Demaret. The L^1 -Potts functional for robust jump-sparse reconstruction. *SIAM Journal on Numerical Analysis*, 53(1):644–673, 2015.
- [119] G. Winkler and V. Liebscher. Smoothers for discontinuous signals. *Journal of Nonparametric Statistics*, 14(1-2):203–222, 2002.
- [120] O. Wittich, A. Kempe, G. Winkler, and V. Liebscher. Complexity penalized least squares estimators: Analytical results. *Mathematische Nachrichten*, 281(4):582–595, 2008.
- [121] G. Xie and T. Yu. Smoothness equivalence properties of general manifold-valued data subdivision schemes. *Multiscale Modeling & Simulation*, 7(3):1073–1100, 2008.